cancels in the *mer* complex. In agreement with this interpretation, the VCD intensities in the CH stretching region of the Λ-*mer* complex, which are lower than those in the Λ-*fac* complex by approximately a factor of 3, correspond in sign and magnitude to that predicted for a single ring in conformation **1**.

We note that the negative CH symmetric stretching VCD feature in the spectrum of Λ-*fac*-Co(β-ala)$_3$ has a weak negative shoulder corresponding to the "A" absorption band. This feature may arise from the coupled oscillator mechanism, which is predicted to result in negative VCD for this band (Figure 2 and Table 1), although it is unclear why a similar feature is absent in the spectrum of the Λ-mer complex. Other CO features are not evident due to partial cancellation and to the large ring current contributions.

The only crystal structure for these complexes that has been reported is for Δ-*mer*-tris(β-alaninato)cobalt(III) tetrahydrate.[17] In the crystal, the ligands were found to have a "twist-boat" conformation, with the sense of twist of one ligand opposite to that of the other two. The conformations of the methylenes correspond to two rings with a δ twist and one with a λ twist; that is, one ring has an opposite twist compared to our proposed solution structure. In the crystal, hydrogen-bonding interactions between amine hydrogens and oxygen atoms on water or on an adjacent complex stabilize the ring conformations. Closer examination of the crystal structure data indicates that for two ligands one NH bond lies within hydrogen-bonding distance (2.3–2.6 Å) and orientation of the coordinated oxygen on an adjacent ligand of the same complex. Such interactions are similar to those we propose in Figure 3 for the complex in solution.

Conclusions

This study of the CH stretching VCD spectra of tris(β-alaninato)cobalt(III) complexes has provided further evidence for the ring current mechanism of VCD, since enhanced VCD intensity can be clearly identified with the modes of "B" symmetry. Only in these modes can the CH stretches generate net current around the ligand ring. Even though the frequencies of the "A" and "B" modes are split, there is little evidence of coupled oscillator contributions, due to the large ring current effects. The VCD spectra of both the Λ-*fac* and Λ-*mer* complexes are consistent with solution conformations stabilized by intramolecular hydrogen bonding between ligands.

Acknowledgment. We acknowledge financial support by grants from the National Institutes of Health (GM-23567) and the National Science Foundation (CHE 86-02854).

Registry No. Λ-*fac*-Co(β-ala)$_3$, 71425-08-6; Λ-*mer*-Co(β-ala)$_3$, 71300-67-9.

Synthesis and Characterization of Novel Flavin-Linked Porphyrins. Mechanism for Flavin-Catalyzed Inter- and Intramolecular 2e/1e Electron-Transfer Reactions[1,2]

Jun Takeda, Shigeru Ohta, and Masaaki Hirobe*

Contribution from the Faculty of Pharmaceutical Sciences, University of Tokyo, Hongo, Bunkyo-ku, Tokyo 113, Japan. *Received December 30, 1986*

Abstract: The synthesis of several flavin-linked porphyrins is described. The two moieties ($Fl_{ox}C_n$(TPP)M, M = H_2 and $Mn^{III}Cl$) are covalently linked by an amide linkage with a methylene spacer group [C_n, n = 1–3] between the ortho position of (*o*-aminophenyl)triphenylporphyrin and the N^3 or N^{10} positions of the flavin. The $Fl_{ox}C_n$(TPP)M (**1a–e**) were characterized by UV–visible, ^{1}H NMR, and IR spectra. The proximity conformation of the flavin and porphyrin ring was demonstrated by ^{1}H NMR studies of $Fl_{ox}C_nTPPH_2$. The electrochemistry of $Fl_{ox}C_n$(TPP)M was investigated by cyclic voltammetry and differential-pulse polarography. Cyclic voltammetry demonstrated that the flavin reduction potentials, $Fl_{ox} + e^- = Fl^{\bullet -}$ and $Fl^{\bullet -} + e^- = Fl^{2-}$, were positively shifted by the proximity of the linked porphyrin moiety. Flavin-catayzed 2e/1e electron-transfer reactions from dihydropyridines to (TPP)$Mn^{III}Cl$ have been investigated kinetically in intermolecular systems (PyH_2 + Fl_{ox} + (TPP)$Mn^{III}Cl$) as well as in intramolecular systems (PyH_2 + $Fl_{ox}C_n$(TPP)$Mn^{III}Cl$) in ethanol solution. In intermolecular systems, the presence of flavin enhances the apparent rates of electron transfer significantly. The kinetic behavior of the intermolecular system is zero order with respect to the (TPP)$Mn^{III}Cl$ concentration and first order with respect to the PyH_2 and Fl_{ox} concentrations, when PyH_2 is in excess and Fl_{ox} is used in 0.25–1.5-fold to (TPP)$Mn^{III}Cl$. These observations indicate that the flavin acts as 2e/1e catalyst. In intramolecular systems, the kinetic behavior differs for the various $Fl_{ox}C_n$(TPP)$Mn^{III}Cl$ systems. Whereas $Fl_{ox}C_1$(TPP)$Mn^{III}Cl$ shows clean first order, $Fl_{ox}C_2$(TPP)$Mn^{III}Cl$ and $Fl_{ox}C_3$(TPP)$Mn^{III}Cl$ exhibit a mixed-order behavior. The apparent second-order rate constants are increased for the intramolecular systems. The rate enhancements by the intramolecular effect are as follows: k_{intra}/k_{inter} = 8.0 (**1a**), 3.9 (**1b**), 2.1 (**1c**), 1.7 (**1d**), and 1.8 (**1e**). These results show that the k_{intra}/k_{inter} values are affected by the methylene spacer length and the linking position. Possible reasons for the rate enhancement are discussed by using electrochemical data, conformational data, and kinetic isotope effects. The proposed reaction mechanism for the intramolecular system, especially for $Fl_{ox}C_1$(TPP)$Mn^{III}Cl$, involves a ternary complex such as [PyH_2···Fl_{ox}···(TPP)$Mn^{III}Cl$]. The described systems are relevant models for biological electron-transfer processes requiring flavin 2e/1e catalysis and for flavin–heme interaction as in flavohemoproteins.

Flavin coenzymes are prosthetic groups in a number of redox proteins and catalyze many types of redox reactions including hydrogen-transfer reactions, electron-transfer reactions, and activation of dioxygen.[3,4] Thus, chemical investigations of the flavin coenzyme have helped considerably in the understanding of enzymatic reaction mechanisms.[4] Unlike the NAD(P)H coenzyme, flavin can readily undergo a one-electron transfer as well as two-electron transfer, since the isoalloxazine ring system has three

(1) Preliminary communication: Takeda, J.; Ohta, S.; Hirobe, M. *Tetrahedron Lett.* **1985**, *26*, 4509–4512.

(2) Takeda, J.; Ohta, S.; Hirobe, M. Presented in part at the 8th IUPAC Conference on Physical Organic Chemistry, Tokyo, Aug 24–29, 1986; Abstracts p 175.

(3) (a) Walsh, C. *Acc. Chem. Res.* **1980**, *13*, 148–155. (b) Walsh, C. In *Enzymatic Reaction Mechanisms*; Freeman: San Francisco, 1979; pp 358–448.

(4) Bruice, T. C. *Acc. Chem. Res.* **1980**, *13*, 256–262, and references therein.

0002-7863/87/1509-7677$01.50/0

accessible redox states: the oxidized (Fl_{ox}), semiquinone (FlH$^{\bullet}$), and reduced (FlH_2) states (eq 1).

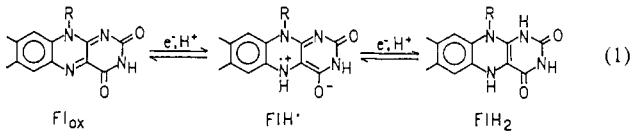

(1)

A broad class of flavoenzymes catalyzes electron-transfer reactions that in effect result in acceptance or donation of a two-electron equivalent from substrates (SH_2/S) such as NAD(P)H, amines, alcohols, and thiols, followed by one-electron transfers from and to redox-active metals ($M^{(n+1)+}/M^{n+}$) like iron in the iron–sulfur core and heme and molybdenum in proteins. The redox reactions of eq 2–4 are illustrative. The ability of flavin to undergo

$$Fl_{ox} + SH_2 \rightleftharpoons FlH_2 + S \quad (2)$$

$$FlH_2 + M^{(n+1)+} \rightleftharpoons FlH^{\bullet} + M^{n+} + H^{+} \quad (3)$$

$$FlH^{\bullet} + M^{(n+1)+} \rightleftharpoons Fl_{ox} + M^{n+} + H^{+} \quad (4)$$

both one-electron and two-electron transfers is exploited in the respiratory chain where flavocoenzymes serve as a redox switch by allowing the changeover between two-electron flow and one-electron flow, the so-called 2e/1e electron-transfer catalysis, to take place. The redox half-reaction of eq 2 has widely been investigated,[3,4] but the electron-transfer process from reduced flavin to metals[5,6] (eq 3 and 4) is not yet sufficiently understood.

Flavin coenzymes coexist with metals in so-called "metalloflavoproteins". Of current interest are approaches that use model systems to study the interaction and mechanism of electron transfer between flavin and metals.[5-11] Hemmerich et al.,[7] in pioneering work of this concern, have shown that oxidized and reduced flavins do not interact easily with metal ions and that the important species is the flavin in the semiquinone state. The electron-transfer reaction between flavin and the iron–sulfur protein is expected to proceed via an inner-sphere mechanism. Fritchie[8] has postulated that the N(5) and O(4′) positions of flavin chelate to the iron atom of the tetrahedral $[Fe_4S_4]$-type ferredoxin in the transient electron-transfer reaction. Recently, ESR studies of flavoenzymes containing an iron–sulfur core, e.g. trimethylamine dehydrogenase, have been interpreted as being suggestive for a direct metal–flavin interaction.[12]

Flavin coenzymes also coexist with heme groups, as found in some microorganisms with heme-containing flavoproteins, so-called "flavohemoproteins", such as cytochrome c_{552} (*Chromatium vinosum*),[13] cytochrome c_{553} (*Chlorobium thiosulfatophilum*),[14] lactate dehydrogenase (aerobic yeast),[15] yeast hemoglobin (*Candida mycoderma*),[16] and an oxygen-binding flavohemoprotein (*Alcaligenos eutrophus*).[17] Electron transfer between flavin coenzymes and heme groups most likely occurs by an outer-sphere mechanism, via π-orbital mixing edge interaction between the benzene ring of the flavin and the porphyrin ring, and not by an inner-sphere mechanism due to steric hinderance between the two ring systems.[18] On the basis of X-ray analysis data, Tollin et al.[19] proposed a transient electron-transfer complex between cytochrome *c* and flavodoxin ("a pure" 1e carrier). The authors have shown that flavin and porphyrin are arranged in a nearly parallel conformation.

In our approach to the problem of the enzymatic electron-transfer reaction mechanism, we present the first flavin-linked porphyrin model systems in which a flavin–heme interaction can be observed.

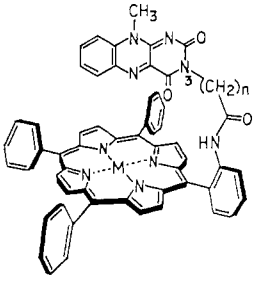

$Fl_{ox}C_nTPPM$

1, M = $Mn^{III}Cl$ 2, M = 2H
a, n = 1
b, n = 2
c, n = 3

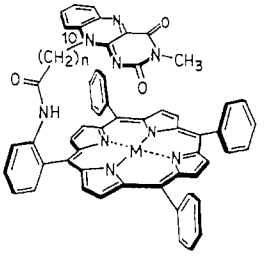

$N^{10}Fl_{ox}C_nTPPM$

1, M = $Mn^{III}Cl$ 2, M = 2H
d, n = 2
e, n = 3

Experimental Section

General Methods. Elemental analyses were performed at the Microanalytical Laboratory at the University of Tokyo. Melting points were determined on a Yanagimoto micro melting point apparatus and are uncorrected. Mass spectra were measured on a JEOL DX-303 mass spectrometer operating in the fast-atom-bombardment (FAB) mode: chloroform (solvent), *p*-nitrobenzyl alcohol (matrix). Infrared spectra were recorded on a Jasco DS-701G spectrophotometer. ^1H NMR spectra were recorded on a Hitachi R-24B (60-MHz) or a JNM FX-100 (100-MHz) pulse Fourier transform NMR spectrometer. Chemical shifts are expressed in units (in ppm) downfield of internal tetramethylsilane. Solvents used are abbreviated as follows: $CDCl_3$, chloroform-*d*; DMSO-d_6, dimethyl-d_6 sulfoxide; TFA, trifluoroacetic acid. Splitting patterns are designated as follows: s, singlet; d, doublet; t, triplet; q, quartet; m, multiplet. Ultraviolet and visible absorption spectra were recorded on a Hitachi 557 double-beam spectrophotometer equipped with thermostatic cell compartments, at temperature of 30 °C.

Materials. All solvents and reagents were of reagent-grade quality, commercially available, and were used without further purification, except when noted. Dimethylformamide (DMF) was treated with 4-Å molecular sieves for several days, distilled under reduced pressure, and stored over 4-Å molecular sieves. Pyridine was refluxed over KOH, distilled, and stored over 4-Å molecular sieves. Ethanol was dried over

(5) (a) Singh, A. N.; Gelerinter, E.; Gould, E. S. *Inorg. Chem.* **1982**, *21*, 1232–1235. (b) Singh, A. N.; Srinivasan, V. S.; Gould, E. S. *Ibid.* **1982**, *21*, 1236–1239.

(6) Favaudon, V.; Lhoste, J.-M. *Biochemistry* **1975**, *14*, 4739–4744.

(7) (a) Bamberg, P.; Hemmerich, P. *Helv. Chim. Acta* **1961**, *44*, 1001–1011. (b) Beinert, H.; Hemmerich, P. *Biochem. Biophys. Res. Commun.* **1965**, *18*, 212–220. (c) Hemmerich, P.; Veeger, C.; Wood, H. C. S. *Angew. Chem., Int. Ed. Engl.* **1965**, *4*, 671–687. (d) Lauterwein, J.; Hemmerich, P.; Lhoste, J.-M. *Inorg. Chem.* **1975**, *14*, 2152–2161. (e) Lauterwein, J.; Hemmerich, P.; Lhoste, J.-M. *Ibid.* **1975**, *14*, 2161–2168.

(8) (a) Fritchie, C. J. *J. Chem. Soc., Chem. Commun.* **1972**, 1220–1222. (b) Fritchie, C. J. *J. Biol. Chem.* **1972**, *247*, 7459–7476. (c) Wade, T. D.; Fritchie, C. J. *Ibid.* **1973**, *248*, 2337–2343. (d) Fritchie, C. J. *Ibid.* **1973**, *248*, 7516–7521. (e) Garland, W. T.; Fritchie, C. J. *Ibid.* **1974**, *249*, 2228–2234.

(9) (a) Clarke, M. J.; Dowling, M. G.; Garafalo, A. R.; Brennan, T. F. *J. Am. Chem. Soc.* **1979**, *101*, 223–225. (b) *J. Biol. Chem.* **1980**, *255*, 3472–3481. (c) Clarke, M. J.; Dowling, M. G. *Inorg. Chem.* **1981**, *20*, 3506–3514. (d) Clarke, M. J.; Dowling, M. G. In *Flavins and Flavoproteins*; Massey, V., Williams, C. H., Eds.; Elsevier North Holland: New York, 1982; pp 579–583. (e) Benecky, M. J.; Dowling, M. G.; Clarke, M. J.; Spiro, T. G. *Inorg. Chem.* **1984**, *23*, 865–869.

(10) (a) Shinkai, S.; Ishikawa, Y.; Manabe, O. *Bull. Chem. Soc. Jpn.* **1983**, *56*, 1694–1699. (b) Shinkai, S.; Honda, N.; Ishikawa, Y.; Manabe, O. *J. Chem. Soc., Perkin Trans. 1* **1985**, 565–573. (c) Shinkai, S.; Honda, N.; Ishikawa, Y.; Müller, F.; Manabe, O. *Chem. Lett.* **1985**, 543–546.

(11) Yano, Y.; Sakaguchi, T.; Nakazato, M. *J. Chem. Soc., Perkin Trans. 2* **1984**, 595–599.

(12) (a) Steenkamp, D. J.; Singer, T. P.; Beinert, H. *Biochem. J.* **1978**, *169*, 361–369. (b) Beinert, H.; Shaw, R. W.; Steenkamp, D. J.; Singer, T. P.; Stevenson, R.; Dunham, W. R.; Sands, R. H. In *Flavins and Flavoproteins*; Massey, V., Williams, C. H., Eds.; Elsevier North Holland: New York, 1982; pp 727–735.

(13) (a) Bartsch, R. G.; Meyer, T. E.; Robinson, A. B. In *Structure and Function of Cytochromes*; Okunuki, K., Kamen, M. D., Sekuzei, I., Eds.; University of Tokyo: Tokyo, 1978; pp 443–451. (b) Strekas, T. C. *Biochim. Biophys. Acta* **1976**, *446*, 179–191. (c) Kitagawa, T.; Fukumori, Y.; Yamanaka, T. *Biochemistry* **1980**, *19*, 5721–5729. (d) Cusanovich, M. A.; Tollin, G. *Ibid.* **1980**, *19*, 3343–3347.

(14) Tollin, G.; Meyer, T. E.; Cusanovich, M. A. *Biochemistry* **1982**, *21*, 3849–3856.

(15) (a) Risler, J.-P. *Biochemistry* **1971**, *10*, 2664–2669. (b) Iwatsubo, M.; Mevel-Ninino, M.; Labeyrie, F. *Ibid.* **1977**, *16*, 3558–3566.

(16) Oshino, R.; Asakura, T.; Takio, K.; Oshino, N.; Chance, B.; Hagihara, B. *Eur. J. Biochem.* **1973**, *39*, 581–590.

(17) Probst, I.; Wolf, G.; Schlegel, H. G. *Biochim. Biophys. Acta* **1979**, *576*, 471–478.

(18) Hemmerich, P. In *Bioinorganic Chemistry II*; Raymond, K. N., Ed.; American Chemical Society: Washington, DC, 1977; pp 312–329.

(19) Simondsen, R. P.; Tollin, G. In *Flavins and Flavoproteins*; Massey, V., Williams, C. H., Eds.; Elsevier North Holland: New York, 1982; pp 719–724.

Na, distilled, and stored over 4-Å molecular sieves. Benzene was distilled and stored over sodium wire. Acetonitrile was refluxed over phosphorus pentoxide, distilled, and stored over 4-Å molecular sieves. Thin-layer chromatography (TLC) was done with precoated silica gel 60-F_{254} (Merck No. 5554) and aluminum oxide 60-F_{254} (Merck No. 5550) sheets with fluorescence indicator. Silica gel for column chromatography was microbead silica gel Grade 4B (100–200 mesh, neutral) purchased from Fuji-Davison Chemical Ltd. Alumina for column chromatography was Merck aluminum oxide 90 (activity II–III, 70–230 mesh).

Porphyrins. *meso*-(*o*-Aminophenyl)triphenylporphyrin (*o*-NH_2TPPH_2) was synthesized by the method of Collman et al.[20] using the mixed condensation of *o*-nitrobenzaldehyde, benzaldehyde, and pyrrole and subsequent reduction by stannous chloride: IR (KBr disk) $\tilde{\nu}$ 963, 796, 726, 628 cm^{-1}; ^1H NMR ($CDCl_3$, 100 MHz) δ −2.75 (s, 2 H, internal py NH), 3.48 (br s, 2 H, NH_2), 7.10, 7.67, and 8.13 (m, 19 H, ArH), 8.28 (m, 8 H, py β-H). *meso*-Tetraphenylporphyrin ($TPPH_2$) was a byproduct in the synthesis of *o*-NH_2TPPH_2. (Tetraphenylporphinato)manganese(III) chloride ((TPP)$Mn^{III}Cl$) was synthesized by the method of Adler et al.[21]

Flavins. 10-Methylisoalloxazine and 3,10-dimethylisoalloxazine (Fl_{ox}) were prepared according to the *N*-oxide method of Yoneda et al.[22] Fl_{ox}: mp (recrystallized from AcOH–H_2O) >300 °C; ^1H NMR (TFA, 60 MHz) δ 3.68 (s, 3 H, N^3-CH_3), 4.60 (s, 3 H, N^{10}-CH_3), 8.38 (m, 4 H, ArH). 7-Chloro-3,10-dimethylisoalloxazine (7-$ClFl_{ox}$) was synthesized by the method of Bruice et al.[23] 7-$ClFl_{ox}$: mp (recrystallized from ethanol–diisopropyl ether) 285–289 °C (lit.[23] mp 295–298 °C); IR (KBr disk) $\tilde{\nu}$ 1708, 1664, 1560, 1268, 1196, 969 cm^{-1}; ^1H NMR ($CDCl_3$, 60 MHz) δ 3.51 (s, 3 H, N^3-CH_3), 4.17 (s, 3 H, N^{10}-CH_3), 7.52 (d, J = 9.6 Hz, 1 H, 9-H), 7.82 (dd, J = 3.0 and 9.6 Hz, 1 H, 8-H), 8.27 (d, J = 3.0 Hz, 1 H, 6-H). Anal. Calcd for $C_{12}H_9N_4O_2Cl$: C, 52.21; H, 3.28; N, 20.25. Found: C, 51.92; H, 3.35; N, 19.99. 7-(Trifluoromethyl)-3,10-dimethylisoalloxazine (7-CF_3Fl_{ox}) was synthesized from 2-chloro-5-(trifluoromethyl)nitrobenzene in the same manner as described for 7-$ClFl_{ox}$: mp (recrystallized from ethanol–diisopropyl ether) 236–238 °C dec; IR (KBr disk) $\tilde{\nu}$ 1706, 1655, 1565, 1365, 1200, 970, 831 cm^{-1}; ^1H NMR ($CDCl_3$, 60 MHz) δ 3.51 (s, 3 H, N^3-CH_3), 4.11 (s, 3 H, N^{10}-CH_3), 7.74 (d, J = 9.6 Hz, 1 H, 9-H), 8.05 (dd, J = 3.0 and 9.6 Hz, 1 H, 8-H), 8.58 (d, J = 3.0 Hz, 1 H, 6-H). Anal. Calcd for $C_{13}H_9N_4O_2F_3$: C, 50.33; H, 2.92; N, 18.06. Found: C, 50.08; H, 3.14; N, 18.16.

Dihydropyridines. *N*-Benzyl-1,4-dihydronicotinamide (BzNADH) was synthesized as described by Mauzerall and Westheimer.[24] 4,4-Dideuterio-*N*-benzyl-1,4-dihydronicotinamide was prepared by the method of Caughey and Schellenberg.[25] The isotopic purity of the deuterio compound was estimated by ^1H NMR analysis and found to be 90% isotopically pure. *N*-Benzyl-1,4-dihydro-2,6-dimethylnicotinamide (2,6-Me_2BzNADH) was available from previous work.[26]

Ethyl 10-Methylisoalloxazine-3-acetate (3a). 10-Methylisoalloxazine (1.00 g, 4.38 mmol) and anhydrous potassium carbonate (3.40 g, 24.6 mmol) were suspended in DMF (200 mL). To this solution was added ethyl bromoacetate (2.80 g, 16.8 mol) and the mixture stirred at room temperature. After 5 h, the reaction solution was filtered, and DMF was removed by rotary evaporation. Water (150 mL) was added to the wet residue, the mixture was extracted with chloroform (150 mL × 3), the combined organic phase was dried over anhydrous sodium sulfate, and the chloroform was removed in vacuo. The yellow residue was recrystallized from ethanol–diisopropyl ether to give fine yellow needles: 1.13 g (82% yield); mp 235–237 °C; IR (KBr disk) $\tilde{\nu}$ 1742, 1710, 1647, 1550, 1208, 1188, 927, 768 cm^{-1}; ^1H NMR ($CDCl_3$, 60 MHz) δ 1.26 (t, J = 7 Hz, 3 H, $CO_2CH_2CH_3$), 4.08 (s, 3 H, N^{10}-CH_3), 4.12 (q, J = 7 Hz, 2 H, $COCH_2$), 4.80 (s, 2 H, N^3-CH_2), 7.60–8.30 (m, 4 H, ArH). Anal. Calcd for $C_{15}H_{14}N_4O_4$: C, 57.32; H, 4.49; N, 17.83. Found: C, 57.12; H, 4.43; N, 17.73.

10-Methylisoalloxazine-3-acetic Acid (4a). The compound **3a** (950 mg, 3.02 mmol) was dissolved in concentrated hydrochloric acid (10 mL) and the resultant mixture stirred at 80–90 °C for 45 min. The reaction mixture was cooled, and ice–water (30 mL) was added to the solution. Yellow crystals that precipitated were collected by suction filtration and washed with water. Recrystallization from 2 N acetic acid gave fine orange needles: 650 mg (70% yield); mp >300 °C; IR (KBr disk) $\tilde{\nu}$ 3040–2300, 1707, 1688, 1545, 1196, 936, 770 cm^{-1}; ^1H NMR (TFA, 60 MHz) δ 4.45 (s, 3 H, N^{10}-CH_3), 4.99 (s, 2 H, N^3-CH_2), 8.1–8.6 (m, 4 H, ArH). Anal. Calcd for $C_{13}H_{19}N_4O_4 \cdot {}^3/_4H_2O$: C, 52.04; H, 3.86; N, 18.76. Found: C, 51.96; H, 3.75; N, 18.74.

10-Methylisoalloxazine-3-acetyl Chloride (5a). Compound **4a** (600 mg, 1.93 mmol) was added to thionyl chloride (6 mL) and the suspension stirred at room temperature. After 10–20 min, **4a** had dissolved, and the solution was stirred for 10 min more. Excess thionyl chloride was removed by rotary evaporation at <40 °C (above 40 °C the product decomposed to an unknown green substance). Last traces of thionyl chloride were removed by repeated evaporation of a benzene solution. The crude acid chloride was used without further purification: IR (Nujol mull) $\tilde{\nu}$ 1795, 1705, 1658, 1572, 1195 cm^{-1}.

Ethyl 10-Methylisoalloxazine-3-propionate (3b). To a suspension of 10-methylisoalloxazine (400 mg, 1.75 mmol) and anhydrous potassium carbonate (2.0 g, 14.5 mmol) in DMF (100 mL) was added ethyl β-bromopropionate (1.58 g, 8.75 mmol). After the reaction mixture was stirred for 5 h at 50 °C, it was poured into water (500 mL) and extracted with chloroform (200 mL × 3). The combined organic phase was washed with water (200 mL × 4) and dried over anhydrous sodium sulfate. Chloroform was removed by rotary evaporation, and the residue was purified by silica gel column chromatography eluting with 1:1 (v/v, %) chloroform–ethyl acetate. The first yellow fraction was collected and concentrated. The residue was recrystallized from ethanol–diisopropyl ether to give fine yellow needles: 145 mg (26% yield); mp 206–207 °C; IR (KBr) $\tilde{\nu}$ 1730, 1710, 1642, 1560, 1183, 767 cm^{-1}; ^1H NMR ($CDCl_3$, 100 MHz) δ 1.34 (t, J = 7 Hz, 3 H, $CO_2CH_2CH_3$), 2.75 (t, J = 7 Hz, 3 H, CH_2CO_2), 4.13 (q, J = 7 Hz, 2 H, CO_2CH_2), 4.14 (s, 3 H, N^{10}-CH_3), 4.42 (t, J = 7 Hz, 2 H, N^3-CH_2), 7.66–8.29 (m, 4 H, ArH). Anal. Calcd for $C_{16}H_{16}N_4O_4$: C, 58.53; H, 4.91; N, 17.07. Found: C, 58.26; H, 4.90; N, 16.97.

10-Methylisoalloxazine-3-propionic Acid (4b). This compound was prepared from **3b**, according to the method for **4a**. The compound **4b**, 64 mg, was obtained from 100 mg of **3b** (70% yield). Recrystallization from ethanol gave fine yellow needles: mp 279–283 °C dec; IR (KBr disk) $\tilde{\nu}$ 3100–2300, 1703, 1630, 1545, 1188, 772 cm^{-1}; ^1H NMR (TFA, 60 MHz) δ 3.01 (m, 2 H, CH_2CO_2), 4.57 (m, 5 H, N^{10}-CH_2), 8.3 (m, 4 H, ArH). Anal. Calcd for $C_{14}H_{12}N_4O_4 \cdot 0.6H_2O$: C, 54.05; H, 4.28; N, 18.01. Found: C, 53.96; H, 3.95; N, 17.78.

10-Methylisoalloxazine-3-propionyl Chloride (5b). This compound was synthesized from **4b** in the same manner as described for **5a**. The yield was almost quantitative as calculated for the hydrochloride salt. The crude acid chloride was used without further pufication: IR (Nujol mull) $\tilde{\nu}$ 1790, 1710, 1640 cm^{-1}.

Ethyl 10-Methylisoalloxazine-3-butyrate (3c). 10-Methylisoalloxazine (1.80 g, 7.88 mmol) and anhydrous potassium carbonate (10.8 g, 79 mmol) were suspended in DMF (200 mL), ethyl γ-bromobutyrate (7.68 g, 39.4 mmol) was added, and the mixture was stirred at 90 °C. After 1 h, the solution became clear. Inorganic salts were filtrated off, and the DMF was removed by rotary evaporation. The yellow residue was purified by column chromatography on silica gel with 1:1 (v/v, %) chloroform–ethyl acetate as eluent. The yellow fraction was collected and evaporated in vacuo. Recrystallization from ethanol–diisopropyl ether gave fine yellow needles: 2.60 g (96% yield); mp 189–191 °C; IR (KBr disk) $\tilde{\nu}$ 1735, 1712, 1646, 1554, 1181, 766 cm^{-1}; ^1H NMR ($CDCl_3$, 100 MHz) δ 1.26 (t, J = 7 Hz, 3 H, $CO_2CH_2CH_3$), 2.08 (m, 2 H, N^3-CH_2CH_2), 2.44 (t, J = 7 Hz, 2 H, CH_2CO_2), 4.14 (m, 7 H, N^{10}-CH_3, N^3-CH_2, and $CO_2CH_2CH_3$), 7.63–8.29 (m, 4 H, ArH). Anal. Calcd for $C_{17}H_{18}N_4O_4$: C, 59.64; H, 5.30; N, 16.37. Found: C, 59.45; H, 5.29; N, 16.09.

10-Methylisoalloxazine-3-butyric Acid (4c). This compound was synthesized in the same manner as the synthesis described for **4a**. Starting from **3c** (1.14 g, 3.33 mmol) gave 740 mg (71% yield) of orange needles after recrystallization from 2 N acetic acid: mp 259–263 °C dec; IR (KBr disk) $\tilde{\nu}$ 3100–2300, 1704, 1640, 1548, 1196, 763 cm^{-1}; ^1H NMR ($CDCl_3$, 100 MHz) δ 2.18 (m, 4 H, $CH_2CH_2CO_2$), 4.18 (m, 5 H, N^3-CH_2 and N^{10}-CH_3), 7.62–8.50 (m, 4 H, aromatic); ^1H NMR (TFA, 60 MHz) δ 2.31 (m, 2 H, CH_2), 2.66 (t, J = 7 Hz, 2 H, CH_2CO_2), 4.34 (t, J = 7 Hz, 2 H, N^3-CH_2), 4.53 (s, 3 H, N^{10}-CH_3), 8.27 (m, 4 H, ArH). Anal. Calcd for $C_{15}H_{14}N_4O_4 \cdot 0.25H_2O$: C, 56.51; H, 4.58; N, 17.57. Found: C, 56.94; H, 4.63; N, 17.21.

10-Methylisoalloxazine-3-butyryl Chloride (5c). This compound was synthesized in the same manner as described for **5a**. The yield was almost quantitative, as calculated for the hydrochloride salt. The yellow powder thus obtained was used without further purification: IR (Nujol

(20) a) Collman, J. P.; Brauman, J. I.; Doxsee, K. M.; Halbert, T. R.; Bunnenberg, E.; Linder, R. E.; La Mar, G. N.; Gaudio, J. D.; Lang, G.; Spartalian, K. *J. Am. Chem. Soc.* **1980**, *102*, 4182–4192. (b) Collman, J. P.; Groh, S. E. *Ibid.* **1982**, *104*, 1391–1403.

(21) Adler, A. D.; Longo, F. R.; Kampas, F.; Kim, J. *J. Inorg. Nucl. Chem.* **1970**, *32*, 2443–2445.

(22) Yoneda, F.; Sakuma, Y.; Ichiba, M.; Shinomura, K. *J. Am. Chem. Soc.* **1976**, *98*, 830–835.

(23) Main, L.; Kasperek, G. J.; Bruice, T. C. *Biochemistry* **1972**, *11*, 3991–4000.

(24) Mauzerall, D.; Westheimer, F. H. *J. Am. Chem. Soc.* **1955**, *77*, 2261–2264.

(25) Caughey, W. S.; Schellenberg, K. A. *J. Org. Chem.* **1966**, *31*, 1978–1982.

(26) Takeda, J.; Ohta, S.; Hirobe, M. *Chem. Pharm. Bull.* **1987**, *35*, 2661–2667.

mull) $\tilde{\nu}$ 1793, 1710, 1642, 1195 cm^{-1}; ^1H NMR (DMSO-d_6) δ 1.92 (m, 2 H, CH_2), 2.26 (t, J = 7 Hz, 2 H, CH_2CO_2), 3.93 (t, J = 7 Hz, 2 H, N^3-CH_2), 3.98 (s, 3 H, N^{10}-CH_3), 7.5–8.4 (m, 4 H, ArH).

o-[N-(2-Cyanoethyl)amino]nitrobenzene. o-Fluoronitrobenzene (8.0 g, 57 mmol) and 2-aminopropionitrile (8.0 g, 114 mmol) in ethanol (50 mL) were refluxed for 5 h and then stirred overnight at room temperature. The orange precipitate formed was collected. The filtrate was concentrated in vacuo, water was added, and the mixture was extracted with dichloromethane. The organic phase was dried over anhydrous sodium sulfate and evaporated in vacuo. The residue thus obtained and the precipitate were combined and recrystallized from ethanol to give orange needles: 10.9 g (80% yield); mp 104–106 °C; ^1H NMR ($CDCl_3$, 60 MHz) δ 2.73 (t, J = 7 Hz, 2 H, CH_2CN), 3.73 (t, J = 7 Hz, 2 H, $NHCH_2$), 6.7–7.5 (m, 4 H, ArH, and NH), 8.17 (dd, J = 2.1 and 8.4 Hz, 1 H, H-6).

o-[N-[2-(Ethoxycarbonyl)ethyl]amino]nitrobenzene (6a). o-[N-(2-Cyanoethyl)amino]nitrobenzene (8.09 g, 4.23 mmol) was suspended in ethanol (300 mL), and dry HCl gas was bubbled through the stirred solution at room temperature. The orange crystals were slowly dissolved as the reaction proceeded (exothermic). After 2 h, the solution was concentrated in vacuo and poured into water (200 mL), and the mixture was neutralized with sodium carbonate, extracted with dichloromethane (200 mL × 2), and dried over anhydrous sodium sulfate. The dichloromethane was removed by rotary evaporation to give an orange oil, which crystallized upon cooling. Recrystallization from ether gave orange crystals: 8.38 g (83% yield); mp 66–68.5 °C; ^1H NMR ($CDCl_3$, 60 MHz) δ 1.27 (t, J = 7 Hz, 3 H, CH_3), 2.64 (t, J = 7 Hz, 2 H, CH_2CO_2), 3.59 (q, 2 H, J = 7 Hz, NH_2CH_2), 4.12 (q, J = 7 Hz, 2 H, CO_2CH_2), 6.6–7.4 (m, 3 H, ArH), 8.13 (dd, J = 1.0 and 8.0 Hz, 1 H, H-6), 7.9–8.3 (br, 1 H, NH).

10-[2-(Ethoxycarbonyl)ethyl]isoalloxazine (7a). The compound **6a** (1.00 g, 4.20 mmol) in methanol (75 mL) was hydrogenated over palladium on charcoal at room temperature until the solution became colorless (320 mL of H_2 was consumed, 282 mL in theory). The resulting reaction mixture was immediately filtered and evaporated in vacuo. The o-phenylenediamine thus obtained was dissolved in acetic acid (10 mL). To this solution were added alloxan monohydrate (810 mg, 5.06 mmol) and boric acid (400 mg, 5.80 mmol) in hot acetic acid (40 mL), and the mixture was stirred for 1 h at room temperature. The reaction mixture turned brown, and a precipitate formed; it was collected and washed with water several times. Recrystallization from chloroform gave fine yellow needles: 824 mg (62% yield); mp 260–265 °C dec; IR (KBr disk) $\tilde{\nu}$ 1725, 1711, 1670, 1547, 1402, 1253, 1025 cm^{-1}; ^1H NMR (DMSO-d_6, 60 MHz) δ 1.17 (t, J = 7 Hz, 3 H, CH_3), 2.77 (t, J = 7 Hz, 2 H, CH_2CO_2), 4.07 (q, J = 7 Hz, 2 H, CO_2CH_2), 4.78 (t, J = 7 Hz, 2 H, N^{10}-CH_2), 7.4–8.3 (m, 5 H, ArH and NH). Anal. Calcd for $C_{15}H_{14}N_4O_4$: C, 57.32; H, 4.49; N, 17.83. Found: C, 56.00; H, 4.35; N, 17.22.

3-Methyl-10-[2-(ethoxycarbonyl)ethyl]isoalloxazine (8a). Methyl iodide (1.0 mL, 2.28 g, 16.1 mmol) was added to a suspension of **7a** (503 mg, 1.60 mmol) and anhydrous potassium carbonate (1.5 g, 10.9 mmol) in DMF (30 mL). The mixture was stirred for 1 h at room temperature and filtered. The filtrate was evaporated in vacuo, and the yellow residue was recrystallized from ethanol to give fine orange needles: 415 mg (79% yield); mp 201–204 °C; IR (KBr disk) $\tilde{\nu}$ 1709, 1657, 1558, 1273, 1212, 1181 cm^{-1}; ^1H NMR ($CDCl_3$, 60 MHz) δ 1.22 (t, J = 7.2 Hz, 3 H, CH_3), 2.90 (t, J = 7.2 Hz, 2 H, CH_2CO_2), 3.44 (s, 3 H, N^3-CH_3), 4.09 (q, J = 7.2 Hz, 2 H, CO_2CH_2), 4.92 (t, J = 7.2 Hz, 2 H, N^{10}-CH_2), 7.4–8.0 (m, 3 H, ArH), 8.20 (dd, J = 1.2 and 8.0 Hz, 1 H, 6-H). Anal. Calcd for $C_{16}H_{16}N_4O_4$: C, 58.53; H, 4.91; N, 17.07. Found: C, 58.49; H, 4.91; N, 17.13.

3-Methylisoalloxazine-10-propionic Acid (9a). Compound **8a** (685 mg, 2.00 mmol) was dissolved in concentrated hydrochloric acid (2 mL) and this solution stirred at 80 °C. After 10 min, a precipitate formed, and stirring was continued 10 min more. After cooling, ice–water (20 mL) was added and the precipitate was collected. Recrystallization from 2 N acetic acid gave fine yellow needles, 512 mg (82% yield).

3-Methylisoalloxazine-10-propionyl Chloride (10a). This compound was synthesized in the same manner as **5a**. The yield was almost quantitative, as calculated for the hydrochloride salt. This yellow powder was used without further purification.

o-[N-[3-(Ethoxycarbonyl)propyl]amino]nitrobenzene (6b). Ethyl γ-aminobutyrate hydrochloride (12.0 g, 71.6 mmol) was dissolved in water (100 mL) and the pH adjusted to 9. The aqueous phase was extracted with dichloromethane (100 mL × 2), the combined organic phase was concentrated in vacuo, and ethanol (50 mL) was immediately added to prevent polymerization. To this solution was added o-fluoronitrobenzene (2.00 g, 14.2 mmol) and the resultant mixture refluxed for 15 h. The reaction mixture was poured into water (200 mL), extracted with dichloromethane (200 mL × 2), and dried over anhydrous sodium sulfate. The solvent was removed by rotary evaporation to give 2.92 g of an orange oil (82% yield). This compound was used directly in subsequent syntheses without further purification: ^1H NMR ($CDCl_3$, 60 MHz) δ 1.24 (t, J = 7.2 Hz, 3 H, CH_3), 2.00 (m, 2 H, CH_2), 2.42 (t, J = 7.2 Hz, 2 H, CH_2CO_2), 3.35 (q, J = 7.2 Hz, 2 H, $NHCH_2$), 6.4–7.5 (m, 3 H, ArH), 8.06 (dd, J = 1.0 and 8.0 Hz, 1 H, H-6), 7.5–8.2 (br, 1 H, HN_2).

10-[3-(Ethoxycarbonyl)propyl]isoalloxazine (7b). This compound was synthesized in the same manner as described for **7a**. Recrystallization from chloroform gave fine yellow needles: 2.70 g (58% yield); mp 258–261 °C; IR (KBr disk) $\tilde{\nu}$ 1725, 1711, 1670, 1547, 1402, 1254, 1182 cm^{-1}; ^1H NMR (DMSO-d_6, 60 MHz) δ 1.17 (t, J = 7.2 Hz, 3 H, CH_3), 1.8–2.7 (m, 4 H, CH_2CH_2), 4.02 (q, J = 7.2 Hz, 2 H, CO_2CH_2), 4.58 (t, J = 7.2 Hz, 3 H, N^{10}-CH_3), 7.3–8.3 (m, 4 H, ArH). Anal. Calcd for $C_{16}H_{16}N_4O_4$: C, 58.53; H, 4.91; N, 17.07. Found: C, 58.26; H, 4.88; N, 17.07.

3-Methyl-10-[3-(ethoxycarbonyl)propyl]isoalloxazine (8b). This compound was synthesized in the same manner as described for **8a**. Starting from **7b** (1.50 g, 4.57 mmol) gave 1.28 g (82% yield) of fine yellow needles after recrystallization from dichloromethane–hexane: mp 238–240 °C; IR (KBr disk) $\tilde{\nu}$ 1719, 1707, 1654, 1560, 1278, 1195 cm^{-1}; ^1H NMR ($CDCl_3$, 60 MHz) δ 1.32 (t, J = 7 Hz, 3 H, CH_3), 2.20 (m, 2 H, CH_2), 2.60 (t, J = 7 Hz, 2 H, CH_2CO_2), 3.50 (s, 3 H, N^3-CH_3), 4.18 (q, J = 7 Hz, 2 H, CO_2CH_2), 4.80 (t, J = 7 Hz, 2 H, N^{10}-CH_2), 7.4–8.3 (m, 4 H, ArH). Anal. Calcd for $C_{18}H_{18}N_4O_4$: C, 59.64; H, 5.30; N, 16.37. Found: C, 59.86; H, 5.34; N, 16.14.

3-Methylisoalloxazine-10-butyric Acid (9b). This compound was synthesized in the same manner as described for **9a**. Starting from **8b** (685 mg, 2.00 mmol) gave 512 mg (82% yield) of fine yellow needles after recrystallization from 2 N acetic acid: mp 268–272 °C dec; IR (KBr disk) $\tilde{\nu}$ 3100–2300, 1709, 1609, 1545, 1286, 770 cm^{-1}; ^1H NMR (TFA, 60 MHz) δ 2.00 (m, 2 H, CH_2), 2.53 (t, J = 7.2 Hz, 2 H, CH_2CO_2H), 3.20 (s, 3 H, N^3-CH_3), 4.60 (t, J = 7.2 Hz, 2 H, N^{10}-CH_2), 8.00 (m, 4 H, ArH). Anal. Calcd for $C_{15}H_{14}O_4N_4 \cdot 0.25H_2O$: C, 56.51; H, 4.58; N, 17.57. Found: C, 56.82; H, 4.58; N, 17.41.

3-Methylisoalloxazine-10-butyryl Chloride (10b). This compound was synthesized in the same manner as described for **5a**. The yield was almost quantitative, as calculated for the hydrochloride salt. The yellow powder was used without further purification: IR (Nujol mull) $\tilde{\nu}$ 1770, 1705, 1612, 1135 cm^{-1}; ^1H NMR (DMSO-d_6, 60 MHz) δ 1.8–2.6 (m, 4 H, methylene), 3.42 (s, 3 H, N^3-CH_3), 4.81 (t, J = 7 Hz, 2 H, N^{10}-CH_2), 7.7–8.4 (m, 4 H, ArH).

General Procedure for the Preparation of the Free Base of the Flavin-Linked Porphyrin. *meso*-[o-(10-Methylisoalloxazine-3-acetamido)phenyl]triphenylporphyrin, $Fl_{ox}C_1TPPH_2$ (2a). A solution of o-NH_2TPPH_2 (600 mg, 0.95 mmol) in DMF (20 mL) containing pyridine (0.5 mL) was added to the solid **5a** (358 mg, 1.05 mmol), and the mixture was stirred under Ar atmosphere and at room temperature. The reaction was followed by observation of TLC (silica gel) patterns and found to be complete within 30 min. The reaction mixture was added to water (250 mL) and extracted with dichloromethane (200 mL × 2); the organic phase was washed with water (200 mL × 6), dried over anhydrous sodium sulfate, and concentrated by rotary evaporation. The crude product was purified by chromatography on silica gel. After a first fraction of o-NH_2TPPH_2 had been eluted with dichloromethane–acetone (95:5, v/v, %), the desired compound was eluted with dichloromethane–acetone (7:3, v/v, %). The purple residue was recrystallized from dichloromethane–hexane to give purple flakes: 485 mg (57% yield); IR (KBr disk) $\tilde{\nu}$ 1695, 1664, 1555, 963, 797, 725 cm^{-1}; ^1H NMR ($CDCl_3$, 100 MHz) δ −3.51 (s, 2 H, internal py NH), 1.54 (br s, 3 H, flavin N^{10}-CH_3), 4.25 (s, 2 H, CH_2), 6.81, 6.85, and 7.0–8.5 (m, 24 H, amide NH and ArH), 8.71 and 8.77 (m, 8 H, py β-H); MS (FAB), m/e 898 $(M + H)^+$; UV–vis characteristics given in Table I. Anal. Calcd for $C_{57}H_{39}N_9O_3 \cdot 3.5H_2O$: C, 71.24; H, 4.82; N, 13.12. Found: C, 71.46; H, 4.45; N, 12.54.

***meso*-[o-(10-Methylisoalloxazine-3-propionamido)phenyl]triphenylporphyrin, $Fl_{ox}C_2TPPH_2$ (2b).** This compound was synthesized from **5b** (59 mg, 0.167 mmol) and o-NH_2TPPH_2 (120 mg, 0.191 mmol) in the same manner as described for **2a**. Recrystallization from dichloromethane–hexane gave a purple solid: 116 mg (76% yield based on **5b**); IR (KBr disk) $\tilde{\nu}$ 1653, 1559, 961, 796, 726 cm^{-1}; ^1H NMR ($CDCl_3$, 100 MHz) δ −3.82 (s, 2 H, internal py NH), 1.25, 1.63, and 3.30 (m, 7 H, methylene and N^{10}-CH_3), 5.20, 6.04, 6.39, and 7.2–8.2 (m, 24 H, amide NH and ArH), 8.71 (m, 8 H, py β-H); MS (FAB), m/e 912 $(M + H)^+$; UV–vis characteristics given in Table I. Anal. Calcd for $C_{58}H_{41}N_9O_3 \cdot 3.5H_2O$: C, 71.44; H, 4.60; N, 12.92. Found: C, 71.62; H, 4.36; N, 12.52.

***meso*-[o-(10-Methylisoalloxazine-3-butyramido)phenyl]triphenylporphyrin, $Fl_{ox}C_3TPPH_2$ (2c).** This compound was synthesized from **5c** (587 mg, 1.59 mmol) and o-NH_2TPPH_2 (700 mg, 1.11 mmol) in the same manner as described for **2a**. Recrystallization from dichloromethane–hexane gave a purple solid: 615 mg (60% yield); IR (KBr disk)

Table I. Absorption Maxima and Extinction Coefficient for the Free Base of Flavin-Linked Porphyrin in Chloroform

	λ_{max}, nm (ϵ, 10^{-3} M^{-1} cm^{-1})					
	UV	Soret	IV	III	II	I
$TPPH_2$		418 (280)	512 (15.5)	548 (6.0)	588 (4.7)	643 (2.8)
$Fl_{ox}C_1TPPH_2$	273 (55.3)	418 (294)	514 (14.4)	548 (6.2)	588 (4.8)	642 (2.6)
$Fl_{ox}C_2TPPH_2$	272 (55.0)	417 (291)	514 (17.3)	548 (6.5)	587 (5.2)	643 (2.6)
$Fl_{ox}C_3TPPH_2$	270 (49.7)	418 (285)	514 (16.1)	548 (6.7)	588 (5.4)	643 (3.3)
N^{10}-$Fl_{ox}C_2TPPH_2$	280 (50.0)	419 (290)	515 (15.8)	550 (6.5)	589 (5.3)	642 (3.0)
N^{10}-$Fl_{ox}C_3TPPH_2$	276 (53.5)	419 (295)	515 (16.5)	549 (6.7)	588 (5.5)	643 (3.1)

$\tilde{\nu}$ 1705, 1656, 1554, 961, 796, 724 cm^{-1}; ^1H NMR ($CDCl_3$, 100 MHz) δ −4.32 (s, 2 H, internal py NH), 0.00, 1.59, 1.73, and 3.08 (m, 9 H, $CH_2CH_2CH_2$ and N^{10}-CH_3), 4.24, 5.40, 6.09, 7.62, and 7.70 (m, amide NH and ArH), 8.42 and 8.55 (m, 8 H, py β-H); MS (FAB), *m/e* 926 $(M + H)^+$; UV–vis characteristics given in Table I. Anal. Calcd for $C_{59}H_{43}N_9O_3 \cdot 2.5H_2O$: C, 72.97; H, 4.98; N, 12.98. Found: C, 72.99; H, 4.69; N, 13.23.

***meso*-[*o*-(3-Methylisoalloxazine-10-propionamido)phenyl]triphenylporphyrin, N^{10}-$Fl_{ox}C_2TPPH_2$ (2d).** This compound was synthesized from **10a** (118 mg, 0.332 mmol) and *o*-NH_2TPPH_2 (250 mg, 0.397 mmol) in the same manner as described for **2a**. Recrystallization from dichloromethane–hexane gave a purple solid: 200 mg (68% yield based on **10a**); IR (KBr disk) $\tilde{\nu}$ 1706, 1655, 1553, 963, 798, 750 cm^{-1}; ^1H NMR ($CDCl_3$, 100 MHz) δ −3.75 (s, 2 H, internal py NH), 0.88, 1.26, and 1.38 (br, 7 H, CH_2CH_2 and N^3-CH_3), 6.47, 7.29, and 7.72 (m, 24 H, amide NH and ArH), 8.50 and 8.62 (m, 8 H, py β-H); MS (FAB), *m/e* 912 $(M + H)^+$; UV–vis characterstics given in Table I. Anal. Calcd for $C_{58}H_{41}N_9O_3 \cdot H_2O$: C, 74.90; H, 4.66; N, 13.55. Found: C, 74.71; H, 4.54; N, 13.58.

***meso*-[*o*-(3-Methylisoalloxazine-10-butyramido)phenyl]triphenylporphyrin, N^{10}-$Fl_{ox}C_3TPPH_2$ (2e).** This compound was synthesized from **10b** (235 mg, 0.636 mmol) and *o*-NH_2TPPH_2 (278 mg, 0.441 mmol) in the same manner as described for **2a**. Recrystallization from dichloromethane–hexane gave a purple solid: 263 mg (65% yield based on *o*-NH_2TPPH_2); IR (KBr disk) $\tilde{\nu}$ 1709, 1655, 1551, 963, 796, 749, 726 cm^{-1}; ^1H NMR ($CDCl_3$, 100 MHz) δ −4.41 (s, 2 H, internal py NH), 1.26 and 2.22 (m, 9 H, methylene and N^3-CH_3), 4.28, 5.62, 7.55, and 7.78 (m, 24 H, amide NH and ArH), 8.36 and 8.96 (m, 8 H, py β-H); MS (FAB), *m/e* 926 $(M + H)^+$; UV–vis characteristics given in Table I. Anal. Calcd for $C_{59}H_{43}N_9O_3 \cdot H_2O$: C, 75.06; H, 4.80; N, 13.35. Found: C, 74.49; H, 4.62; N, 13.33.

General Procedure for the Preparation of the Manganese(III)–Chloro Complexes of the Flavin-Linked Porphyrin. Manganese(III) complexes were prepared by a modified procedure of Adler et al.[21] The free base of a flavin-linked porphyrin (450 mg) dissolved in DMF (20 mL) and the resultant mixture heated at 130 °C. $Mn(OAc)_2 \cdot 4H_2O$ (100 mg) was added to the solution. After 15 min, a second portion of $Mn(OAc)_2 \cdot 4H_2O$ (100 mg) was added and the reaction checked by TLC (alumina, dichloromethane). If free base still remained, a third portion of $Mn(OAc) \cdot 4H_2O$ was added. Reaction times varied from 0.5 to 2 h. DMF was removed by rotary evaporation at 75–85 °C, and the greenish residue was dissolved in dichloromethane and purified by chromatography on alumina. Remaining starting material was first eluted with dichloromethane, and then the product (green band) was eluted with dichloromethane–methanol (18:1, v/v, %). The latter fraction was washed with 0.1 N HCl saturated with NaCl (100 mL × 2) and then dried over NaCl. The green residue was recrystallized from dichloromethane–hexane to give a green powder.

[*meso*-[*o*-(10-Methylisoalloxazine-3-acetamido)phenyl]triphenylporphinato]manganese(III) chloride, $Fl_{ox}C_1(TPP)Mn^{III}Cl$ (1a): UV–vis (EtOH) λ_{max} (ϵ, 10^{-3} M^{-1} cm^{-1}) 216 (75), 264 (65), 378 (61), 399 (65), 466 (115), 510 (8), 564 (13), 598 (9).

[*meso*-[*o*-(10-Methylisoalloxazine-3-propionamido)phenyl]triphenylporphinato]manganese(III) chloride, $Fl_{ox}C_2(TPP)Mn^{III}Cl$ (1b): UV–vis (EtOH) λ_{max} (ϵ) 216 (73), 262 (61), 378 (60), 399 (64), 466 (109), 512 (8), 564 (13), 597 (9).

[*meso*-[*o*-(10-Methylisoalloxazine-3-butyramido)phenyl]triphenylporphinato]manganese(III) chloride, $Fl_{ox}C_3(TPP)Mn^{III}Cl$ (1c): UV–vis (EtOH) λ_{max} (ϵ) 216 (73), 262 (61), 378 (58), 399 (64), 466 (112), 512 (8), 564 (13), 597 (9).

[*meso*-[*o*-(3-Methylisoalloxazine-10-propionamido)phenyl]triphenylporphinato]manganese(III) chloride, N^{10}-$Fl_{ox}C_2(TPP)Mn^{III}Cl$, (1d): UV–vis (EtOH) λ_{max} (ϵ) 215 (74), 258 (60), 378 (60), 399 (64), 466 (110), 512 (8), 562 (13), 596 (9).

[*meso*-[*o*-(3-Methylisoalloxazine-10-butyramido)phenyl]triphenylporphinato]manganese(III) chloride, N^{10}-$Fl_{ox}C_3(TPP)Mn^{III}Cl$ (1e): UV–vis (EtOH) λ_{max} (ϵ) 224 (72), 264 (62), 378 (61), 398 (61), 466 (116), 564 (13), 600 (9).

Demetalation of $Fl_{ox}C_1(TPP)Mn^{III}Cl$ (1a). Manganese(III) complex of flavin-linked porphyrin **1a** (20 mg) in ethanol (2 mL) and BzNADH (50 mg) in ethanol (2 mL) were mixed under Ar atmosphere. The reaction mixture was allowed to stand for 2 h at room temperature. As the reaction proceeded, the brown solution (Mn^{III} in EtOH) turned to a light green solution (Mn^{II} in EtOH). Upon addition of concentrated HCl (ca. 0.1 mL) by needle under Ar atmosphere, the reaction mixture immediately turned dark green (diprotonated free-base porphyrin). After several minutes, the reaction mixture was extracted with a chloroform (50 mL) and water (50 mL) mixture, and the chloroform phase was washed with water (50 mL × 3). The only product by TLC (silica gel) was **2a**. The chloroform phase was dried over anhydrous sodium sulfate and concentrated in vacuo. The residue was purified by silica gel column chromatography. The ^1H NMR spectrum ($CDCl_3$) of the product was identical with that of **2a**.

Electrochemical Measurements. These were carried out with a Yanagimoto P-1000 voltammetric analyzer and with a cylic voltammetric circuit. Cyclic voltammograms were recorded on a Watanabe X-Y recorder. A standard three-electrode cell employing platinum (for cyclic voltammetry) or dropping mercury (for differential-pulse polarography) working electrodes and a counter electrode with an SCE reference electrode were used. All of the solutions were prepared at 1 mM and contained 0.1 M tetraethylammonium perchlorate (TEAP) as a supporting electrolyte. All operations for electrochemical studies were carried out under an atmosphere of Ar and with Ar-purged solutions. All potentials, unless otherwise noted, are given vs SCE.

Kinetic Measurements for the Inter- and Intramolecular Electron-Transfer Reactions. All kinetic runs were followed by UV–vis spectrometry at 30 ± 0.2 °C in modified Thunberg cuvettes. In a typical experiment, 2 mL of $Fl_{ox}C_n(TPP)Mn^{III}Cl$ stock solution (2×10^{-5} M in ethanol) was placed in the bottom part of the cuvette and 2 mL of a stock solution of dihydropyridine (>2×10^{-4} M in ethanol) was placed in the upper arm of the cuvette. Both solutions were deaerated by bubbling prehumidified Ar gas for 20 min. After the cuvette was equilibrated at 30 °C, the reaction was initiated by mixing the contents of the cuvette. The reaction was followed by monitoring of the disappearance of Mn(III) moiety (466 nm in ethanol). For the intermolecular electron-transfer reaction, the procedures were the same except that 1 mL of Fl_{ox} stock solution (4×10^{-5} M in ethanol) and 1 mL of $(TPP)Mn^{III}Cl$ stock solution (4×10^{-5} M in ethanol) were placed in the bottom part of the cuvette.

Kinetic Measurements for the Reduction of Flavin by BzNADH. The rate for the reduction of flavin by BzNADH was followed by UV–vis spectrometry at 30 ± 0.2 °C in modified Thunberg cuvettes. The decrease of the flavin absorption maxima (Fl_{ox}, 433 nm; 7-$ClFl_{ox}$, 442 nm; 7-CF_3Fl_{ox}, 428 nm in EtOH) obeyed pseudo-first-order kinetics up to 6 half-lives under the condition that [BzNADH] ≫ [Fl_{ox}]. The pseudo-first-order rate constants were proportional to the [BzNADH] for all the flavins. The procedures were similar to those used for the intermolecular electron-transfer reaction except for the absence of $(TPP)Mn^{III}Cl$.

Product Study. BzNADH (50 mg) and the flavin-linked porphyrin **1a** (20 mg) were dissolved in ethanol (20 mL) and stirred overnight under air. The reaction was quenched by 1 N HCl (0.5 mL) and extracted with a chloroform (50 mL) and water (50 mL) mixture. The aqueous phase was washed with chloroform–2-propanol (7:3, v/v, %; 50 mL × 2). The aqueous phase was evaporated in vacuo. The ^1H NMR spectrum (D_2O) of the residue was identical with that of *N*-benzylnicotinamide.

Results and Discussion

Synthesis of Flavin-Linked Porphyrins. Several linked coenzymes containing the flavin moiety have been synthesized to investigate flavin–flavin,[27] flavin–nicotinamide,[28] and flavin–

(27) (a) Leonard, N. J.; Lambert, R. F. *J. Org. Chem.* **1969**, *34*, 3240–3248. (b) Yano, Y.; Ohya, E. *Chem. Lett.* **1983**, 1281–1284. (c) Yano, Y.; Ohya, E.; Kawabara, Y. *Ibid.* **1984**, 1009–1012. (d) Yano, Y.; Ohya, E. *J. Chem. Soc., Perkin Trans. 2* **1984**, 1227–1232. (e) Zipplies, M. F.; Staab, H. A. *Tetrahedron Lett.* **1984**, *25*, 1035–1038.

Scheme I

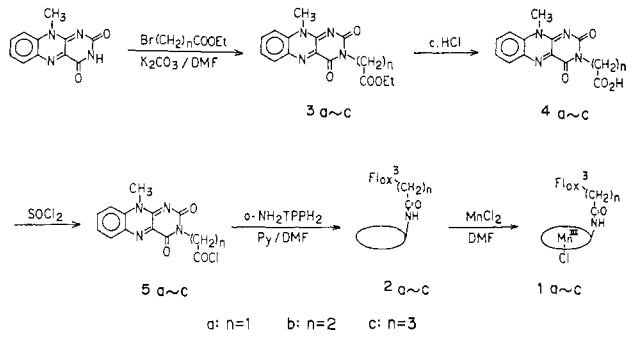

Scheme II

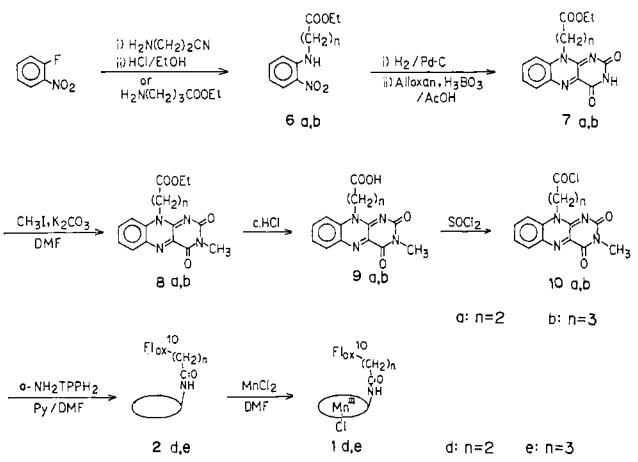

thiazolium[29] redox interactions. A methylene spacer group, attached at the positions N^3, N^{10}, or C^6 of the isoalloxazine ring system, has been used to covalently link the two coenzymes. For this investigation, we chose to link the porphyrin to the N^3 and N^{10} positions of the isoalloxazine ring.

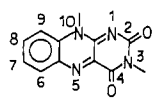

The porphyrin part, (*o*-aminophenyl)triphenylporphyrin, was prepared by Collman's method.[20] The synthetic route to flavin-linked porphyrins is shown in Scheme I. The flavin carboxylic acid **4**, which was required to link the flavin moiety, was obtained as follows. 10-Methylisoalloxazine was alkylated with ethyl bromoacetate (n = 1), ethyl β-bromopropionate (n = 2), and ethyl γ-bromobutyrate (n = 3), respectively, and potassium carbonate in DMF. In the case of n = 1 and 3, the alkylation proceeded readily and gave the ester **3** in good yield. However, the alkylation with ethyl β-bromopropionate gave the ester in low yield, probably due to the instability of the ethyl β-bromopropionate in the basic medium. Because of the instability of the isoalloxazine ring in strongly alkaline media,[30] the hydrolysis of the ethyl ester was performed in concentrated HCl at 80–90 °C. Attempts to condense the flavin carboxylic acids **4** and *o*-NH_2TPPH_2 with dicyclohexylcarbodiimide, carbonyl diimidazolide, and diphenylphosphoryl azide were unsuccessful, probably as a result of steric hindrance of the *o*-amino group. Thus, we chose a condensation via the flavin acid chlorides **5**, which were easily prepared from

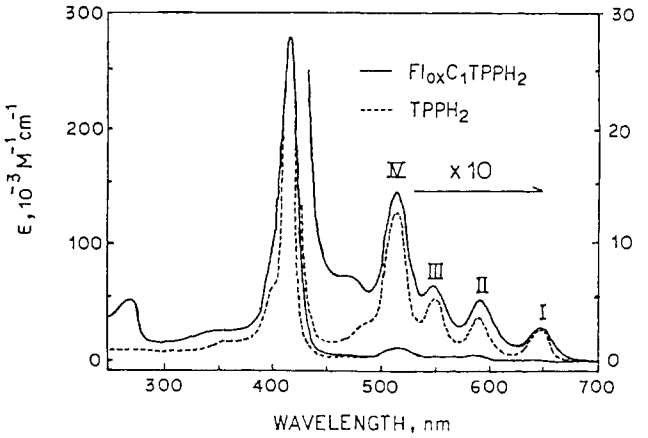

Figure 1. UV–vis spectra of $Flox C_1TPPH_2$ (—) and $TPPH_2$ (---) in chloroform. The expanding spectra (×10) were also shown in the 450–700-nm region.

Table II. Selected ^1H NMR Chemical Shifts for the Free Base of Flavin-Linked Porphyrin in $CDCl_3$ at 24 °C

	δ^a ($\Delta\delta$)^b	
	internal py NH	py β-H
o-NH_2TPPH_2	−2.75	8.82, 8.86
$Flox C_1TPPH_2$	−3.51 (0.76)	8.71, 8.77 (0.10)
$Flox C_2TPPH_2$	−3.82 (1.07)	8.71 (0.13)
$Flox C_3TPPH_2$	−4.32 (1.57)	8.42, 8.55 (0.38)
N^{10}-$Flox C_2TPPH_2$	−3.75 (1.00)	8.50, 8.62 (0.28)
N^{10}-$Flox C_3TPPH_2$	−4.41 (1.66)	8.36, 8.69 (0.33)

$^a\delta$ values were expressed downfield of internal TMS. $^b\Delta\delta$ values were expressed as follows: $\Delta\delta = \delta(o\text{-}NH_2TPPH_2) - \delta(Flox C_nTPPH_2)$.

the acids **4** with thionyl chloride and were stable isolatable derivatives whose purity could be determined by IR and ^1H NMR spectroscopies.

The flavin acid chlorides **5** and *o*-NH_2TPPH_2 were coupled to form the flavin-linked porphyrins in DMF. Addition of a small amount of dry pyridine was effective in each case. The condensation reaction proceeded readily at room temperature and reached completion within 30 min. It was easily followed by TLC. The products were easily isolated and purified by silica gel chromatography. By this method, we could synthesize flavin-linked porphyrins with three different methylene chain lengths, **2a** (n = 1), **2b** (n = 2), and **2c** (n = 3), in their free-base form. N^{10}-Flavin-linked porphyrins, **2d** (n = 2) and **2e** (n = 3), were synthesized in a similar manner from the flavin-10-carboxylic acids, which were prepared as shown in Scheme II. The free bases were characterized by IR, UV–visible, FAB–mass, and ^1H NMR spectroscopies (see below) and elemental analysis. Manganese(III) insertion was carried out with $Mn(OAc)_2$ in DMF at 130 °C, and the products were purified by column chromatography on alumina. It was confirmed by demetalation of the reduced form of compound **1a** (reduced by BzNADH) with HCl that no decomposition of the flavin-linked porphyrin had occurred during the metalation process.[31]

Spectroscopic Properties of Flavin-Linked Porphyrins. (a) UV–Visible Spectra. UV–visible spectra of the flavin-linked porphyrins and $TPPH_2$ are listed in Table I, and typical spectra are shown in Figure 1. These data indicate that UV–visible spectra of flavin-linked porphyrins are very similar to that of $TPPH_2$ except for a band at 280 nm and a shoulder at 460 nm, which originates from the flavin moiety. The shapes of the Soret and visible bands are noticeably broadened. These broadenings of the absorption bands of flavin-linked porphyrins may be due to the close proximity of the two chromophores. Similar results have been observed in the case of quinone-linked porphyrins.[32]

(28) (a) Proffitt, R. T.; Ingraham, L. L.; Blankenhorn, G. *Biochim. Biophys. Acta* **1974**, *362*, 534–548. (b) Blankenhorn, G. *Eur. J. Biochem.* **1975**, *50*, 351–356.

(29) (a) Shinkai, S.; Yamashita, T.; Manabe, O. *Chem. Lett.* **1981**, 961–964. (b) Shinkai, S.; Yamashita, T.; Kusano, Y.; Manabe, O. *J. Am. Chem. Soc.* **1982**, *104*, 563–568.

(30) (a) Smith, S. B.; Bruice, T. C. *J. Am. Chem. Soc.* **1975**, *97*, 2875–2881. (b) Harayama, T.; Tezuka, Y.; Taga, T.; Yoneda, F. *Tetrahedron Lett.* **1984**, *25*, 4015–4018.

(31) It is known that manganese(II) porphyrins can easily be demetalated under acidic conditions. See: Carnieri, N.; Harriman, A.; Porter, G.; Kalyanasundaram, K. *J. Chem. Soc., Dalton Trans.* **1982**, 1231–1238.

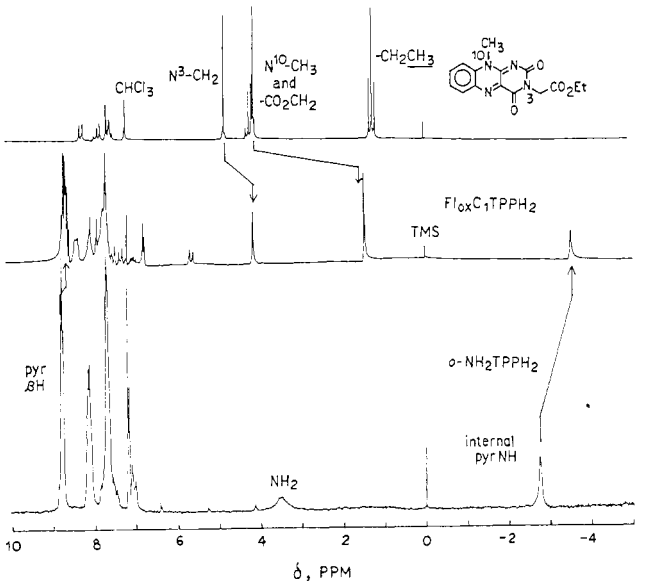

Figure 2. 100-MHz ^{1}H NMR spectra of ethyl 10-methylisoalloxazine-3-acetate, $Fl_{ox}C_1TPPH_2$ (**2a**), and *o*-NH_2TPPH_2 in $CDCl_3$ at 24 °C.

The manganese(III) complexes of the flavin-linked porphyrins and its fully reduced state (reduced by $NaBH_4$ under Ar) in EtOH gave spectra similar to those of the corresponding Mn–TPP complex. Hence, no perturbation in the UV–visible spectrum of the porphyrin resulting from the covalently linked flavin moiety could be observed.

(b) ^{1}H NMR Spectra of the Free-Base Form. Since signal broadening in the ^{1}H NMR spectra of manganese(III) porphyrin by the magnetic anisotropic effect has been known,[33] we measured the ^{1}H NMR spectra of the flavin-linked porphyrin free bases. In contrast to UV–visible spectra, ^{1}H NMR data provide information about the geometry of the flavin-linked porphyrin. ^{1}H NMR data for the flavin-linked porphyrins are listed in Table II, and the ^{1}H NMR spectra of the flavin-linked porphyrin **2a** and its reference compound in $CDCl_3$ are shown in Figure 2. These data show a significant upfield shift of the internal pyrrole NH and pyrrole β-H signals by a shielding effect of the ring current of the closely linked flavin ring system. Similarly, a pronounced upfield shift for the flavin N^{10}-methyl and -methylene spacer proton shifts, which result from the ring current effects of the porphyrin macrocycle, can be observed. Changes in the chemical shift caused by the diamagnetic anisotropy of the porphyrin ring system are well-known, the magnitudes of these changes depending directly on the distance from ring center.[34] Note that the internal pyrrole NH proton signals of N^{10}-$Fl_{ox}C_3TPPH_2$ (**2e**) are shifted 1.66 ppm vs the corresponding signal of *o*-NH_2TPPH_2 and are the most strongly shifted ones. It is interesting that the upfield shifts of the internal pyrrole NH proton signals are affected by the methylene spacer length and the linking position, demonstrating a difference in geometry. Especially noteworthy is the fact that the flavin aromatic proton signals, for which a detailed assignment could not be made, were also shifted with respect to the signals of the precursor flavin ester derivatives.

The NMR spectra of the flavin-linked porphyrins provide inconclusive, but suggestive, data about the stereochemical nature of these compounds. Since large shifts were observed, the flavin ring system seems to be located closely above the porphyrin ring system.

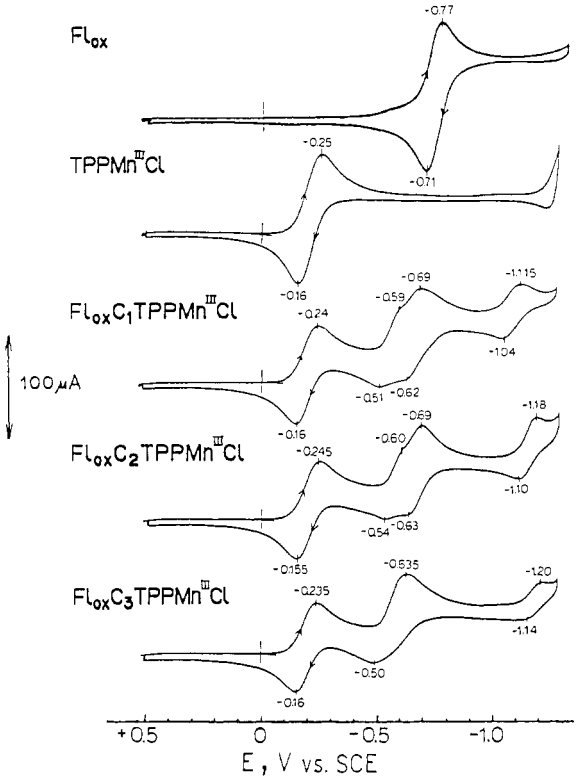

Figure 3. Cyclic voltammograms of Fl_{ox} (3,10-dimethylisoalloxazine), (TPP)$Mn^{III}Cl$, and $Fl_{ox}C_n$(TPP)$Mn^{III}Cl$ in DMF containing 0.1 M TEAP as supporting electrolyte. All the concentrations were about 1 mM. Sweep rate was 10 mV/s.

Stacking in the flavin–porphyrin molecule in various conformations was examined with CPK (Corey–Pauling–Koltun) molecular models. The considered conformations show a distance of about 5–7 Å between the two parallel ring systems and fit the ^{1}H NMR data. We assume that the amide proton is close to either the flavin O(2′) or O(4′) atom and hydrogen bonding is possible. Such a hydrogen bond is common in flavin chemistry.

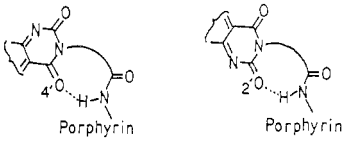

Electrochemistry. Electrochemical data of the flavin-linked porphyrins gave useful information about the interaction between flavin and manganese(III) porphyrin and porphyrin free base, respectively. Electrochemical investigations were carried out with cyclic voltammetry (Pt working electrode) or differential-pulse polarography (dropping-Hg working electrode) in DMF and CH_3CN containing 0.1 M tetraethylammonium perchlorate as supporting electrolyte. Differential-pulse polarography of the flavin-linked porphyrin free base **2a** produced three reduction waves with half-wave potentials of −0.73, −1.07, and −1.41 V (data are not shown in figure). The redox potentials of the flavin reference compound (3,10-dimethylisoalloxazine) are of almost the same value (−0.74, −1.31 V). Redox potentials of $TPPH_2$ were −1.08 and −1.46 V (data are not shown in figure). These results suggest that the redox potential of flavin-linked porphyrin free base at −0.73 V corresponds to the $Fl_{ox}/Fl^{\bullet-}$ couple and the second wave at −1.07 V to the $TPPH_2/TPPH_2^{\bullet-}$ couple. The third wave at −1.41 V would result from mixing of the two redox reactions ($Fl^{\bullet-}/Fl^{2-}$ and $TPPH_2^{\bullet-}/TPPH_2^{2-}$). This fact also suggests negligible interaction between flavin and porphyrin free-base moiety in DMF. However, differential-pulse polarography of **2a** in acetonitrile (a less polar solvent relative to DMF) showed the redox potentials at −0.74, −1.11, −1.38, and −1.55 V, where the potentials of 3,10-dimethylisoalloxazine, determined to −0.82 and −1.39 V, indicated a flavin–porphyrin interaction. The positive shift of the

(32) (a) Tabushi, I.; Koga, N.; Yanagita, M. *Tetrahedron Lett.* **1979**, 257–260. (b) Dalton, J.; Milgrom, L. R. *J. Chem. Soc., Chem. Commun.* **1979**, 609–610. (c) Lindsey, J. S.; Mauzerall, D. C.; Linschitz, H. *J. Am. Chem. Soc.* **1983**, *105*, 6528–6529. (d) Nishitani, S.; Kurata, N.; Sakata, Y.; Misumi, S.; Karen, A.; Okada, T.; Mataga, N. *Ibid.* **1983**, *105*, 7771–7772. (e) Wasielewski, M. R.; Niemczyk, M. P. *Ibid.* **1984**, *106*, 5043–5045.

(33) La Mar, G. N.; Walker, F. A. *J. Am. Chem. Soc.* **1975**, *97*, 5103–5107.

(34) Seheer, H.; Katz, J. J. In *Porphyrin and Metalloporphyrins*; Smith, K. M., Ed.; Elsevier: New York, 1975; pp 399–524.

Table III. Voltammetric Data of Flavin-Linked Porphyrins[a]

	$E_{1/2}$,[b] V vs SCE (ΔE_p, mV)		
	Mn^{III}/Mn^{II}	$Fl_{ox}/Fl^{\bullet-}$	$Fl^{\bullet-}/Fl^{2-}$
Fl_{ox}		−0.74 (60)	−1.31[c]
(TPP)$Mn^{III}Cl$	−0.21 (90)		
$Fl_{ox}C_1$(TPP)$Mn^{III}Cl$	−0.20 (80)	−0.655 (70)	−1.07 (70)
$Fl_{ox}C_2$(TPP)$Mn^{III}Cl$	−0.20 (90)	−0.66 (60)	−1.14 (80)
$Fl_{ox}C_3$(TPP)$Mn^{III}Cl$	−0.21 (75)	−0.635[d]	−1.17 (60)
N^{10}-$Fl_{ox}C_2$(TPP)$Mn^{III}Cl$	−0.19 (80)	−0.64[d]	−1.24 (50)
N^{10}-$Fl_{ox}C_3$(TPP)$Mn^{III}Cl$	−0.19 (90)	−0.72 (60)	−1.21 (65)

[a] Measured about 1 mM DMF solution containing 0.1 M TEAP at Pt electrode. [b] Halfe-wave potential, $E_{1/2}$, was calculated from $E_{1/2} = (E_a + E_c)/2$. [c] Irreversible process and cathodic peak potential were shown. [d] Quasi-reversible (chemically reversible) process and cathodic peak potential were shown (see Figure 3).

redox potential for $Fl_{ox}/Fl^{\bullet-}$ in acetonitrile suggests an interaction between flavin and porphyrin moieties. In DMF such a complexation does not occur due to solvation of the two chromophores.

Unlike the flavin-linked porphyrin free base, cyclic voltammetry of manganese(III) flavin-linked porphyrin in DMF exhibits a strong flavin–manganese(III) porphyrin interaction. Cyclic voltammograms for (TPP)$Mn^{III}Cl$, Fl_{ox}, and $Fl_{ox}C_n$(TPP)$Mn^{III}Cl$ are shown in Figure 3. Introduction of manganese(III) into the flavin-linked porphyrin leads to a redox wave of approximately −0.2 V vs SCE, which is typical for the Mn^{III}/Mn^{II} redox couple of (TPP)$Mn^{III}Cl$.[35] It is interesting that the second redox wave ($Fl_{ox}/Fl^{\bullet-}$ couple) is shifted positively about 0.02–0.11 V (e.g. for the case of $Fl_{ox}C_1$(TPP)$Mn^{III}Cl$, the actual couple values being referred to −0.62/−0.69 V) compared with 3,10-dimethylisoalloxazine. The third redox wave corresponding to the $Fl^{\bullet-}/Fl^{2-}$ couple is also positively shifted. Furthermore, the $Fl^{\bullet-}/Fl^{2-}$ couple shows quasi-reversible properties (eq 7), whereas this step in 3,10-dimethylisoalloxazine is completely irreversible (eq 5). No

$$Fl_{ox} \rightleftharpoons Fl^{\bullet-} \rightarrow Fl^{2-} \quad (5)$$

$$(TPP)Mn^{III+} \rightleftharpoons (TPP)Mn^{II} \quad (6)$$

$$\overline{Fl_{ox}\ (TPP)Mn^{III+}} \rightleftharpoons \overline{Fl_{ox}\ (TPP)Mn^{II}} \rightleftharpoons \overline{Fl^{\bullet-}\ (TPP)Mn^{II}} \rightleftharpoons \overline{Fl^{2-}\ (TPP)Mn^{II}} \quad (7)$$

interaction can be observed when 1 equiv of 3,10-dimethylisoalloxazine is added to a solution of (TPP)$Mn^{III}Cl$. In Table III, the half-wave potentials, $E_{1/2}$, and the peak separations for the manganese flavin-linked porphyrins as well as reference compounds are summarized. As mentioned above the flavin and the manganese porphyrin moieties show no strong interaction in their all-oxidized forms in UV–visible spectra. However, it is clear from Table III that the flavin and the porphyrin moieties interact to produce the positive shifts.

To the best of our knowledge, only two electrochemical studies of flavin–metal interaction have been reported. Sawyer et al.[36,37] investigated the effects of various metal ions on the properties of electrochemically produced flavin semiquinone and pyocyanine semiquinone, a flavin-like compound. The authors have shown that flavin semiquinone and metal ions, such as Fe^{II}, form a complex that induces a positive shift of the $Fl_{ox}/Fl^{\bullet-}$ couple and a great peak separation in DMSO solution. In another study,[9] where flavin was coordinated on its N(5) and O(4′) positions of the isoalloxazine ring to Ru(II), electrochemical reduction proceeds through two successive single-electron steps, due to destabilization of the fully reduced flavin in aqueous solution as well as in DMF. Moreover, the redox potential of $Fl_{ox}/Fl^{\bullet-}$ couple is negatively shifted because of metal to ligand charge transfer.

Intermolecular Electron Transfer. Reduction of (TPP)$Mn^{III}Cl$ by 1,4-dihydropyridines in ethanol is too slow to investigate its kinetics. In the presence of flavin, the apparent rates of (TPP)$Mn^{III}Cl$ reduction are significantly enhanced, the flavin acting in the important role of an electron carrier between BzNADH (2e reductant) and (TPP)$Mn^{III}Cl$ (1e oxidant). Thus, we investigated the flavin-catalyzed intermolecular electron-transfer reaction. The reactions were carried out in ethanol solution containing 3,10-dimethylisoalloxazine (Fl_{ox}, 0.25–1.5 × 10^{-5} M), (TPP)$Mn^{III}Cl$ (1 × 10^{-5} M), and a large excess amount of the 1,4-dihydropyridines under Ar atmosphere and at 30 °C. In these systems, rates of reaction were determined by monitoring the disappearance of (TPP)$Mn^{III}Cl$ at 466 nm (eq 8). Changes in

$$PyH_2 + (TPP)Mn^{III} \xrightarrow{Fl_{ox}} PyH^+ + (TPP)Mn^{II} \quad (8)$$

the visible spectra from 400 to 600 nm were consistent with the formation of (TPP)Mn^{II} (λ_{max} = 432 nm) and had tight isosbestic points, indicating no accumulation of the flavin semiquinone species. Introduction of air regenerated (TPP)$Mn^{III}Cl$ quantitatively. In all cases the disappearance of (TPP)$Mn^{III}Cl$ obeyed the pseudo-zero-order rate law up to 80–90% conversion and changed to first order with respect to [(TPP)$Mn^{III}Cl$] at the second stage of the reaction. The time courses of the reactions ($(A_0 - A_t)/(A_0 - A_\infty)$ vs time at A_{466}) are plotted in Figure 4. These results indicate that the intermolecular electron-transfer reaction

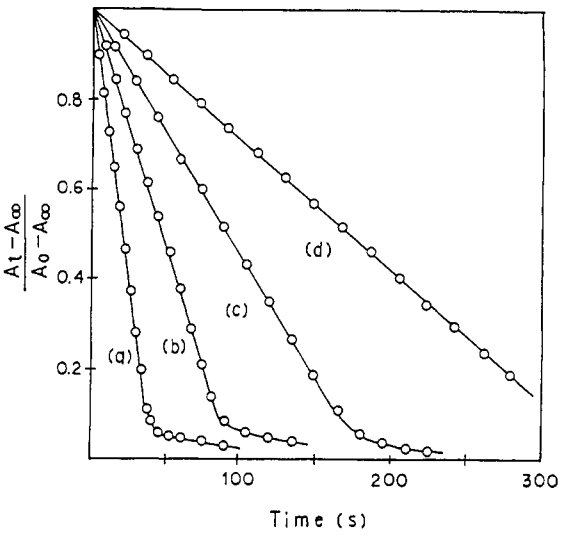

Figure 4. Time course [$(A_t - A_\infty)/(A_0 - A_\infty)$ vs time] plots for the intermolecular electron-transfer reaction in ethanol at 30 °C under Ar atmosphere: [(TPP)$Mn^{III}Cl$] = [Fl_{ox}] = 1 × 10^{-5} M; [BzNADH] = 12.1 (a), 8.07 (b), 6.06 (c), and 3.03 × 10^{-3} M (d).

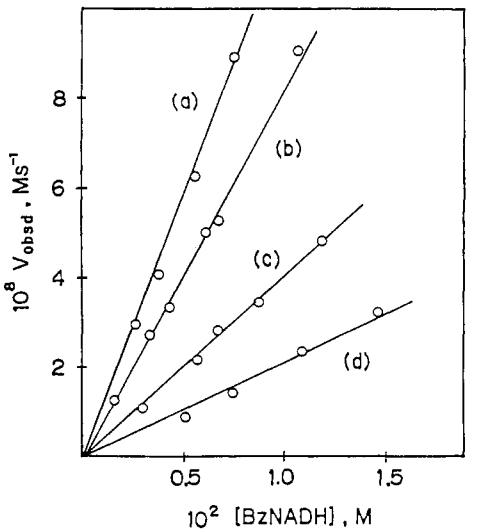

Figure 5. Dependence of v_{obsd} upon [BzNADH] for the intermolecular electron-transfer reaction: [Fl_{ox}] = 1.5 (a), 1.0 (b), 0.5 (c), and 0.25 × 10^{-5} M (d).

(35) Kelly, S. L.; Kadish, K. M. *Inorg. Chem.* **1982**, *21*, 3631–3639.
(36) Sawyer, D. T.; McCreery, R. L. *Inorg. Chem.* **1972**, *11*, 779–782.
(37) (a) Morrison, M. M.; Seo, E. T.; Howie, J. K.; Sawyer, D. T. *J. Am. Chem. Soc.* **1978**, *100*, 207–211. (b) Morrison, M. M.; Sawyer, D. T. *Ibid.* **1978**, *100*, 211–213.

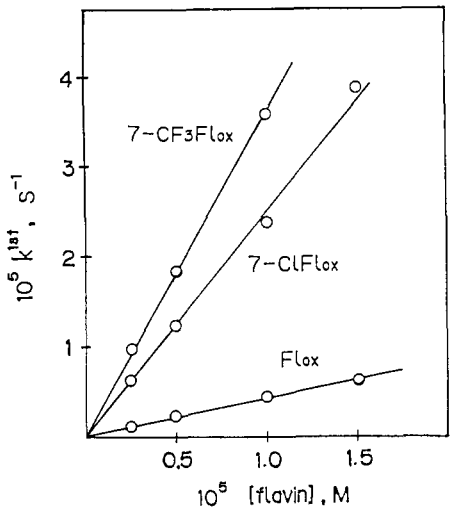

Figure 6. Dependence of k^{1st} (v_{obsd}/[BzNADH]) upon [Fl_{ox}] for the intermolecular electron-transfer reaction.

is independent of [(TPP)$Mn^{III}Cl$], when [PyH_2]$_0$ ≫ [Fl_{ox}]$_0$ ~ [(TPP)$Mn^{III}Cl$]. Thus the experimentally obtained rate expression can be written as eq 9.

$$V = \text{constant} \times [PyH_2]_0 \times [Fl_{ox}]_0 \quad (9)$$

The values of the apparent zero-order rate constants (v_{obsd}) were taken from the slopes of Figure 4. The pseudo-zero-order rate constants (v_{obsd}) depend linearly on [PyH_2]$_0$ (Figure 5), and furthermore, the slopes of Figure 5 (k^{1st}) depend linearly on [Fl_{ox}]$_0$ (Figure 6). Thus, we obtain the apparent second-order rate constant (k^{2nd}) of 0.794 M^{-1} s^{-1}. Reactions using a different 1,4-dihydropyridine, 2,6-Me_2BzNADH, show the same kinetic behavior, with a k^{2nd} of 36.2 M^{-1} s^{-1}. The most reasonable kinetic scheme that fits the results involves a rate-determining step prior to the (TPP)$Mn^{III}Cl$ reduction step (Scheme III). The rate-

Scheme III

$$PyH_2 + Fl_{ox} \rightleftharpoons PyH_2\cdots Fl_{ox} \xrightarrow{k_2} PyH^+ + FlH^- \quad (10)$$

$$FlH^- + (TPP)Mn^{III+} \xrightarrow{k_3} FlH^\bullet + (TPP)Mn^{II} \quad (11)$$

$$FlH^\bullet + (TPP)Mn^{III+} \xrightarrow{k_4} Fl_{ox} + (TPP)Mn^{II} + H^+ \quad (12)$$

determining step in this system should be the 2e reduction of Fl_{ox} by PyH_2 (eq 10) whereas the 1e transfer from FlH^- and $FlH^\bullet$, respectively, to (TPP)Mn^{III+} is supposed to be very fast (see below). From Scheme III, when [FlH^-] and [$FlH^\bullet$] are at steady state, the pseudo-zero-order rate constant (v_{obsd}) for disappearance of (TPP)Mn^{III+} is expressed by eq 13, where [Fl_{ox}]$_0$ = [Fl_{ox}] +

$$v_{obsd} = -\frac{d[Mn^{III+}]}{dt} = \frac{2k_2[PyH]_0[Fl_{ox}]_0}{1 + \left(\frac{k_3 + k_4}{k_3k_4}\right)k_2\left(\frac{[PyH]_0}{[(TPP)Mn^{III}]}\right)} \quad (13)$$

[$FlH^\bullet$] + [FlH^-]. The second term of the denominator will decrease as the reaction proceeds but dominate the kinetics up to 80% conversion. Thus, the second term of the denominator can be neglected, and we obtain eq 14, which indicates a zero-order

$$v_{obsd} = 2k_2[PyH_2]_0[Fl_{ox}]_0 \quad (14)$$

$$k^{2nd} = 2k_2;\ k^{1st} = k^{2nd}[PyH_2]_0$$

rate constant with respect to [(TPP)Mn^{III+}] and is consistent with eq 9. Close to completion of the reaction, the second term in the denominator of eq 13 cannot be neglected and the disappearance of (TPP)Mn^{III+} obeys eq 15, which represents the second phase

$$v_{obsd} = (2k_3k_4/k_3 + k_4)[Fl_{ox}]_0[(TPP)Mn^{III+}] \quad (15)$$

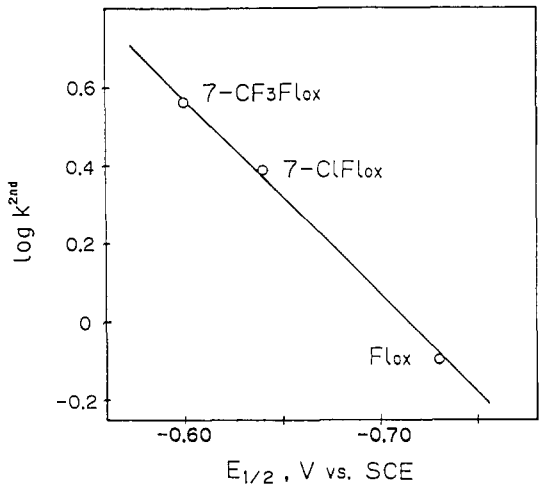

Figure 7. Plot of the logarithm of k^{2nd} for the intermolecular electron-transfer reaction catalyzed by various flavin vs the $E_{1/2}$ (in DMF) of the flavin.

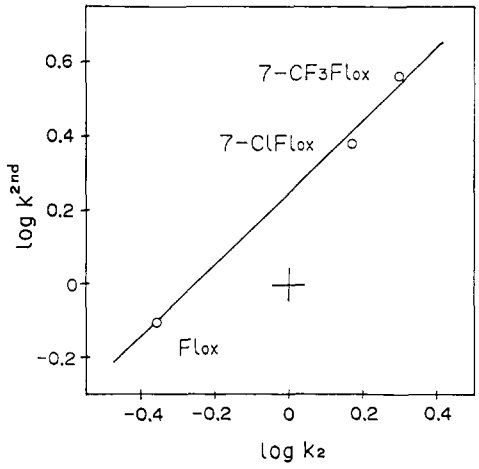

Figure 8. Plot of the correlation between log k^{2nd} (BzNADH + flavin + (TPP)$Mn^{III}Cl$) and log k_2 (BzNADH + flavin). Both of the reactions were carried out in ethanol at 30 °C under Ar atmosphere.

of the reaction (pseudo-first-order decay of (TPP)Mn^{III+}). The mechanism proposed in Scheme III involves a catalytic process where flavin carries the electrons from the 1,4-dihydropyridine to the porphyrin. Such a mechanism is also supported by results of experiments with 7-ClFl_{ox} and 7-CF_3Fl_{ox}, high-potential flavins ($E_{1/2}$ = −0.64 and −0.60 V, respectively, in DMF). A plot of

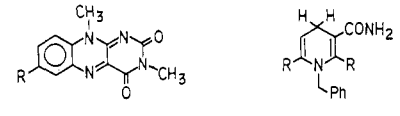

log k^{2nd} vs $E_{1/2}$ was found to be linear (Figure 7) and can be expressed by eq 16 as found by least-squares analysis (γ = 0.965).

$$\log k^{2nd} = 4.99E_{1/2} + 3.56 \quad (16)$$

The dependence of the apparent second-order rate constants on the $E_{1/2}$ of the flavins indicates that the reduction of flavin by BzNADH (eq 10) is involved in the rate-determining step. The kinetic isotope effects (k_H/k_D = 4.60, see below) also support the mechanism proposed in Scheme III. To verify the relationship of $k^{2nd} = 2k_2$ (eq 14), we independently investigated the reduction of the flavin by BzNADH. In Figure 8, log k^{2nd} vs log k_2 for the reduction of flavin by BzNADH is plotted. The graph is linear (γ = 0.997) with slope of unity (0.98) and an intercept of 0.25,

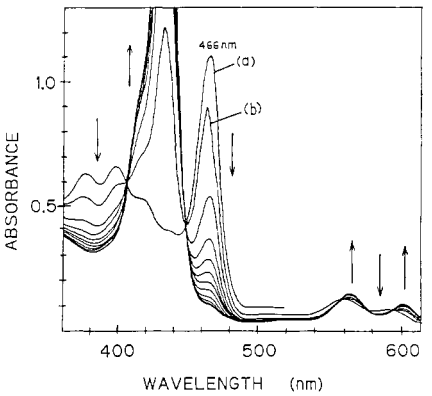

Figure 9. Repetitive scan of the intramolecular electron-transfer reaction of **1** (1×10^{-5} M) and 2,6-Me_2BzNADH (5×10^{-5} M) in ethanol at 30 °C under Ar atmosphere: (a) spectrum of (TPP)M^{III}Cl, (b) scan immediately after mixing, and subsequent spectra were taken at 1-min interval. Scan speed was 300 nm/min.

which indicates the $k^{2nd} = 10^{0.25}k_2$ (=1.78k_2) (eq 17). The value of 1.78 is almost in accordance with the expected value of 2 in eq 14.

$$\log k^{2nd} = 0.98 \log k_2 + 0.25 \quad (17)$$

Bruice et al.[38] have reported a similar flavin catalysis in the 2e/1e electron-transfer reaction between a series of 1,4-dihydropyridines and the 1,10-ethano-5-ethyllumiflavinium radical. They attributed their results, the pseudo-zero-order disappearance of 1,10-ethano-5-ethyllumiflavinium radical, to the catalysis by 1,10-ethano-5-ethyllumiflavinium cation, which was present as a trace impurity.

Intramolecular Electron Transfer. In the flavin-linked porphyrins, **1a–e**, this was investigated under almost the same conditions as used for the intermolecular system. Reaction rates were determined by following the disappearance of the absorption at 466 nm, which directly reflects the reduction of the Mn^{III} porphyrin moiety. Repetitive scanning from 400 to 650 nm revealed tight isosbestic points and, therefore, no accumulation of flavin semiquinone species. Repetitive visible scans of a typical reaction, the reaction of $Fl_{ox}C_1$(TPP)Mn^{III}Cl and 2,6-Me_2BzNADH, are shown in Figure 9.

The reaction of **1a** and BzNADH followed pseudo-first-order kinetics up to 3 half-lives (Figure 10A), and the observed pseudo-first-order rate constants, k_{obsd}, were directly proportional to the BzNADH concentration. Thus, we obtained the apparent second-order-rate constant, $k^{2nd} = 6.36$ M^{-1} s^{-1}.

The kinetics for the reaction of **1b** and **1d** with BzNADH could not be fitted to either first-order or zero-order decay curves. The semilogarithmic plots [ln $[(A_0 - A_\infty)/(A_t - A_\infty)]$ vs time] showed increasing deviations from the first-order rate law (Figure 10B). Thus, we determined the pseudo-order rate constants from the initial rate. This initial rate was linearly dependent upon the BzNADH concentration, and from the slope of this plot, we obtained the second-order rate constant. In the case of **1c** and **1e**, the reaction obeyed the pseudo-first-order law up to only 2 half-lives (Figure 10C). The second-order rate constants obtained from both initial rate and pseudo-order rate laws were consistent within experimental error. The dependence of k_{obsd} on [BzNADH] is shown in Figure 11.

In Table IV, the second-order rate constants for the inter- and intramolecular electron-transfer reaction are summarized. The reaction rates are enhanced by the intramolecular effect. The acceleration factors, k_{intra}/k_{inter}, are 8.0 for **1a**, 3.9 for **1b**, 2.1 for **1c**, 1.7 for **1d**, and 1.8 for **1e**. This shows that the rate for the intramolecular reaction as well as the kinetic behavior greatly depends on the length of the flexible methylene spacer group and the linking position.

(38) Powell, M. F.; Bruice, T. C. *J. Am. Chem. Soc.* **1983**, *105*, 1014–1021.

Table IV. Apparent Second-Order Rate Constants (k^{2nd}) for the Inter- and Intramolecular Electron-Transfer Reaction with BzNADH in Ethanol at 30 °C

system	k^{2nd}, M^{-1} s^{-1}	k_{intra}/k_{inter}
Fl_{ox} + (TPP)Mn^{III}Cl	0.794 ± 0.029[a]	
$Fl_{ox}C_1$(TPP)Mn^{III}Cl	6.36 ± 0.20[b]	8.0
$Fl_{ox}C_2$(TPP)Mn^{III}Cl	3.07 ± 0.13[b]	3.9
$Fl_{ox}C_3$(TPP)Mn^{III}Cl	1.66 ± 0.03[b]	2.1
N^{10}-$Fl_{ox}C_2$(TPP)Mn^{III}Cl	1.32 ± 0.10[b]	1.7
N^{10}-$Fl_{ox}C_3$(TPP)Mn^{III}Cl	1.42 ± 0.09[b]	1.8

[a] k^{2nd} was calculated as the slope of Figure 6. [b] k^{2nd} was calculated from the slope of Figure 11.

Mechanisms for the Intramolecular Electron-Transfer System. Two mechanisms for the intramolecular electron-transfer reaction, which are described in Schemes IV and V, were considered. The mechanism in Scheme IV involves two one-electron transfers from the 1,4-dihydropyridine (e, H^+, e or e, H• transfer). Such a mechanism has been postulated for the reaction of a 1,4-dihydropyridine with one-electron oxidants such as ferricyanide and spirocyclohexylporphyrexide[39] but is only seen in cases of high potential one-electron oxidants ($E° > 600$ mV vs NHE, i.e. 0.36 V vs SCE). With the low redox potential of (TPP)Mn^{III}Cl ($E_{1/2}$ = −0.2 V vs SCE), the reaction seems unlikely to occur by this mechanism. Even if the one-electron oxidation potential of the 1,4-dihydropyridine were lowered by ligation to the metal, the mechanism in Scheme IV is unfavorable, because the electron transfer from the 1,4-dihydropyridine to manganese(III) is thermodynamically disadvantageous.[40] Furthermore, spectra did not indicate a ligation of PyH_2 to (TPP)Mn^{III+} in our system (ethanol solvent).[41,42]

Scheme IV

$$PyH_2 + \overline{Fl_{ox}\ (TPP)Mn^{III+}} \rightleftharpoons \overline{Fl_{ox}\ (TPP)Mn^{III+}}\cdots PyH_2$$

$$\overline{Fl_{ox}\ (TPP)Mn^{III+}}\cdots PyH_2 \rightarrow \overline{Fl_{ox}\ (TPP)Mn^{II}}\cdots PyH^\bullet + H^+$$

$$\overline{Fl_{ox}\ (TPP)Mn^{II}}\cdots PyH^\bullet \rightarrow \overline{FlH^-\ (TPP)Mn^{II}} + PyH^+$$

Scheme V

$$PyH_2 + \overline{Fl_{ox}\ (TPP)Mn^{III+}} \rightleftharpoons PyH_2\cdots\overline{Fl_{ox}\ (TPP)Mn^{III+}}$$

$$PyH_2\cdots\overline{Fl_{ox}\ (TPP)Mn^{III+}} \rightarrow PyH^+\cdots\overline{FlH^-\ (TPP)Mn^{III+}} \rightarrow PyH^+ + \overline{FlH^-\ (TPP)Mn^{III+}}$$

$$\overline{FlH^-\ (TPP)Mn^{III+}} \rightarrow \overline{FlH^\bullet\ (TPP)Mn^{II}}$$

$$\overline{FlH^\bullet\ (TPP)Mn^{II}} + \overline{Fl_{ox}\ (TPP)Mn^{III+}} \rightarrow 2\overline{Fl_{ox}\ (TPP)Mn^{II}} + H^+$$

To gain further information about the reaction mechanism, the kinetic isotope effect was measured with BzNADH-*4,4-d*$_2$ (90% deuterium enriched). The observed kinetic isotope effect (k_H'/k_D') was calculated from the ratio of the k^{2nd} values for the protio and deuterio substrates. The corrected kinetic isotope effect (k_H/k_D)

(39) (a) Blankenhorn, G. *Eur. J. Biochem.* **1976**, *67*, 67–80. (b) Fukuzumi, S.; Kondo, Y.; Tanaka, T. *J. Chem. Soc., Perkin Trans. 2* **1984**, 673–679.

(40) The reported redox potential of $PyH_2/PyH_2^{\bullet+}$ couple is about 0.56–0.76 V vs SCE (the original value is given vs NHE) and too high to reduce manganese(III) moiety (−0.2 V). See: Carlson, B. W.; Miller, L. L.; Neta, P.; Grodkowski, J. *J. Am. Chem. Soc.* **1984**, *106*, 7233–7239, and references therein.

(41) We detected the visible spectra change prior to the redox reaction in the more apolar solvent acetonitrile. This change was probably due to the ligation of BzNADH to (TPP)Mn^{III}Cl.

(42) The ligation of BzNADH to (TPP)$Fe^{III}ClO_4$ was reported by: Fukuzumi, S.; Kondo, Y.; Tanaka, T. *J. Chem. Soc., Chem. Commun.* **1985**, 1053–1054.

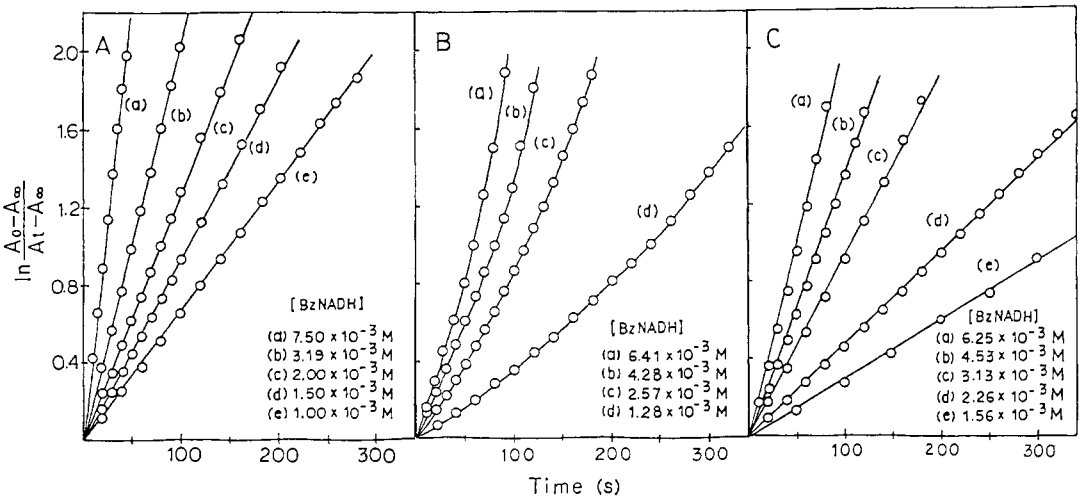

Figure 10. First-order plots [ln $((A_0 - A_\infty)/(A_t - A_\infty))$ vs time] for the intramolecular electron-transfer reaction of BzNADH with (A) **1a**, (B) **1b**, and (C) **1c** in ethanol at 30 °C under Ar atmosphere.

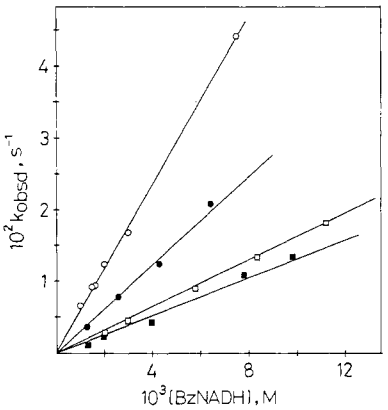

Figure 11. Dependence of pseudo-first-order rate constant (k_{obsd}) upon [BzNADH]. Key: (○) **1a**, (●) **1b**, (□) **1c**, and (■) **1d**. For the case of **1e**, the plot was omitted for clarity. The k_{obsd} for **1b** was calculated as initial velocity/$[\mathbf{1b}]_0$.

Table V. Summary of the Kinetic Isotope Effects for the Inter- and Intramolecular Electron-Transfer Reaction with BzNADH and BzNADH-*4,4*-d_2[a] in Ethanol at 30 °C

system	k_H'/k_D'[b]	k_H/k_D[c]
Fl_{ox} + (TPP)$Mn^{III}Cl$	3.38	4.60
$Fl_{ox}C_1$(TPP)$Mn^{III}Cl$	2.65 ± 0.14	3.24
$Fl_{ox}C_2$(TPP)$Mn^{III}Cl$	2.90 ± 0.18	3.68
$Fl_{ox}C_3$(TPP)$Mn^{III}Cl$	2.97 ± 0.17	3.80

[a] From the ^1H NMR integration, 90% deuterium enriched in the 4-position. [b] Observed kinetic isotope effect calculated from the ratio of k^{2nd} for BzNADH and BzNADH-*4,4*-d_2. [c] Corrected kinetic isotope effect calculated on the assumption that secondary kinetic effect was unity.[43]

was calculated on the basis of the assumption that secondary kinetic isotope effects equal unity.[43] In Table V, the kinetic isotope effects for the inter- and intramolecular systems are summarized. For the intermolecular system, $k_H/k_D = 4.60$ is a commonly found value for the reaction of flavin with 1,4-dihydropyridines.[38,44] The value strongly supports the mechanism proposed in the intermolecular system (Scheme III). The k_H/k_D values for the intramolecular system are somewhat small compared with the ones of the intermolecular system, but they are sufficient to exclude the mechanism shown in Scheme IV.

The kinetic behavior and the k_H/k_D values support the reaction sequence shown in Scheme V, which includes as rate-determining step the reduction of the flavin moiety by the 1,4-dihydropyridine. The rate expression for Scheme V (eq 18) was obtained by the

$$v = -\frac{d[Mn^{III+}]}{dt} = 2k_2[PyH_2]_0[Fl_{ox}C_n(TPP)Mn^{III}Cl] \qquad (18)$$

steady-state assumption with respect to $[\overline{FlH^-\ (TPP)}Mn^{III}]$ and $[\overline{FlH^\bullet\ (TPP)}Mn^{II}]$. It shows a first-order reaction with respect to both $[PyH_2]_0$ and $[Fl_{ox}C_n(TPP)Mn^{III+}]$ and fits the kinetics of the reaction of **1a** well. The reaction of **1b** seems not to obey the pseudo-first-order rate law and is accompanied by increasing deviations. This is probably due to autocatalytic processes such as in eq 19 and 20.

$$\overline{FlH^-\ (TPP)}Mn^{III+} + \overline{Fl_{ox}\ (TPP)}Mn^{III+} \rightarrow \overline{FlH^\bullet\ (TPP)}Mn^{III+} + \overline{Fl_{ox}\ (TPP)}Mn^{II} \qquad (19)$$

$$\overline{FlH^\bullet\ (TPP)}Mn^{III+} \rightarrow \overline{Fl_{ox}\ (TPP)}Mn^{II} + H^+ \qquad (20)$$

Determination of the exact kinetics for the intramolecular system is difficult, because many redox states of flavin-linked manganese porphyrin (six redox forms are possible) are able to participate in the reaction.

Some of the data may explain the observed rate acceleration in the intra- vs the intermolecular case. The redox potentials of the $Fl_{ox}/Fl^{\bullet-}$ couple for $Fl_{ox}C_n$(TPP)$Mn^{III}Cl$ are positively shifted by about $E_{1/2}$ = 0.02–0.11 V as compared to 3,10-dimethylisoalloxazine. Moreover, the Fl^-/Fl^{2-} couple is also positively shifted. These data indicate a stabilization of the semiquinone and the fully reduced state of flavin in the proximity of the Mn–porphyrin. The positive shift of $E_{1/2}$ should accelerate the rate of the reaction by k_{intra}/k_{inter} = 1.3–3.5.[45] This factor, however, is too low to explain the observed rate accelerations, especially the one for the reaction of **1a**.

The rates for the redox reaction between flavin and NADH model compounds have been correlated to polarographically determined $E_{1/2}$ of the $Fl_{ox}/FlH^{\bullet-}$ (H_2O) couple[44,46,47] and to steric

(43) The corrected kinetic isotope effect (k_H/k_D) was calculated from $k_H/k_D = 0.9k_H^{2nd}/(k_D^{2nd} - 0.1k_H^{2nd}) = 0.9(k_H'/k_D')/(1 - 0.1(k_H'/k_D'))$.

(44) The intermolecular electron-transfer reaction between BzNADH with (TPP)$Mn^{III}Cl$ catalyzed by three flavins showed that the log k_2 was linearly related to $E_{1/2}$ (DMF) and the slope (log $k_2/E_{1/2}$) was 4.99 V^{-1} (see eq 16). We expected the acceleration factor from the relationship $k_{intra}/k_{inter} = 10^{4.99E_{1/2}}$.

(45) (a) Porter, D. J. T.; Blankenhorn, G.; Ingraham, L. L. *Biochem. Biophys. Res. Commun.* **1973**, *52*, 447–452. (b) Suelter, C. H.; Metzler, D. E. *Biochim. Biophys. Acta* **1960**, *44*, 23–33.

(46) (a) Bruice, T. C.; Main, L.; Smith, S.; Bruice, P. Y. *J. Am. Chem. Soc.* **1971**, *93*, 7325–7328. (b) Blankenhorn, G. *Biochemistry* **1975**, *14*, 3172–3176.

(47) (a) Gascoigne, I. M.; Radda, G. K. *Biochim. Biophys. Acta* **1967**, *131*, 498–507. (c) Gumbley, S. J.; Main, L. *Tetrahedron Lett.* **1976**, 3209–3212. (d) Shinkai, S.; Honda, N.; Ishikawa, Y.; Manabe, O. *J. Am. Chem. Soc.* **1985**, *107*, 6286–6292.

Scheme VI

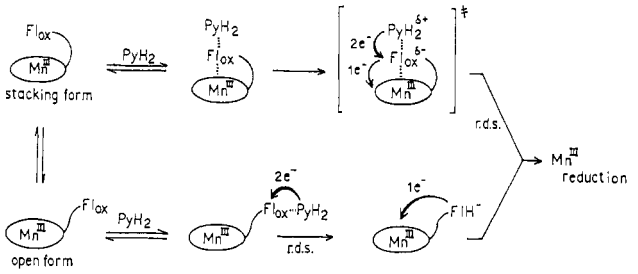

factors.[46] For the flavin-linked porphyrins the one-electron redox potentials are not correlated to the log k^{2nd}, but we assume that geometrical factors play an important role. The methylene chain length considerably affects the chemical shifts in the ^1H NMR spectra, which reflect the geometry of the flavin-linked porphyrin. In kinetic studies, we used the polar and protic solvent ethanol for practical reasons. In this solvent the flavin moiety is probably partly solvated, and the stability of the stacked conformation decreases with an increase of the flexible methylene chain length. The intermediate state clearly reflects the initial conformation. $Fl_{ox}C_1(TPP)Mn^{III}Cl$, which has little freedom around the methylene spacer, is in a more folded conformation than **1b** and **1c**, and the reaction should proceed via a ternary complex $[PyH_2\cdots Fl_{ox}\cdots(TPP)Mn^{III+}]$. It has been well-known that the redox reaction between flavin and a 1,4-dihydropyridine proceeds via a preequilibrium charge-transfer-type complex $[PyH_2\cdots Fl_{ox}]$.[46] In the proposed ternary complex, one electron can be rapidly transferred to the near manganese(III) porphyrin. The reaction of **1b**, **1c**, **1d**, and **1e** proceeds only partly via this ternary complex and mostly via its open form. The proposed reaction mechanism is summarized in Scheme VI.

Conclusion. Novel flavin-linked porphyrins have been synthesized. The key step, the condensation of the flavin carboxylic acid and the *o*-NH_2TPPH_2, which was carried out via the flavin acid chloride, proceeds in good yield. Spectrophotometric studies revealed that the flavin and the porphyrin moieties are in close proximity in the all-oxidized form. Electrochemical studies suggest an interaction of the chromophores in redox reactions. Especially, the potentials of the $Fl_{ox}/Fl^{\bullet-}$ and $Fl^{\bullet-}/Fl^{2-}$ couples are significantly shifted to more positive values. The flavin-catalyzed 2e/1e electron-transfer reactions between NADH model compounds and $(TPP)Mn^{III}Cl$ were investigated in intermolecular systems (Fl_{ox} + PyH_2 + $(TPP)Mn^{III}Cl$) as well as in intramolecular systems ($Fl_{ox}C_n(TPP)Mn^{III}Cl$ + PyH_2). Reaction rates were accelerated by the intramolecular effect, and this acceleration was strongly affected by the methylene spacer length and the linking position.

Synthesis, Structure, and Alkylation of Chiral Vinylrhenium Complexes (η^5-C_5H_5)Re(NO)(PPh_3)(CX=CHR) (X = H, OCH_3). A Mechanistic Study of 1,3-Asymmetric Induction from Rhenium to Carbon

Gerardo S. Bodner,[1] Danny E. Smith,[1] William G. Hatton,[1] Poh Choo Heah,[1] Savas Georgiou,[1] Arnold L. Rheingold,*[2] Steven J. Geib,[2] John P. Hutchinson,[1] and J. A. Gladysz*[1]

Contribution from the Departments of Chemistry, University of Utah, Salt Lake City, Utah 84112, and University of Delaware, Newark, Delaware 19716. *Received March 17, 1987*

Abstract: Reaction of alkylidene complexes $[(\eta^5\text{-}C_5H_5)Re(NO)(PPh_3)(=CHCH_2R)]^+PF_6^-$ (**1**-PF_6^-; **a**, R = H; **b**, R = CH_3; **c**, R = $CH_2CH_2CH_3$; **d**, R = $CH_2C_6H_5$) with DBU or *t*-BuO^-K^+ gives vinyl complexes (*E*)-(η^5-C_5H_5)Re(NO)(PPh_3)(CH=CHR) ((*E*)-**2a-d**; 72-86%). Complexes (*E*)-**2b-d** equilibrate to 84-92:16-8 *E*/*Z* mixtures in solution. Complex (*E*)-**2b** reacts with CF_3SO_3H and CH_3OSO_2F to give ethylidene complex **1b**-$CF_3SO_3^-$ and isobutylidene complex $[(\eta^5\text{-}C_5H_5)Re(NO)(PPh_3)(=CHCH(CH_3)_2)]^+FSO_3^-$ (**3**-FSO_3^-; ca. 65%) and with CF_3SO_3D and CD_3OSO_2F to give mainly (*SR,RS*)-**1b**-β-*d*-$CF_3SO_3^-$ and (*SS,RR*)-$[(\eta^5\text{-}C_5H_5)Re(NO)(PPh_3)(=CHCH(CH_3)(CD_3))]^+FSO_3^-$. However, experimental problems hinder quantification of the 1,3-asymmetric induction. Reaction of **3**-FSO_3^- and *t*-BuO^-K^+ gives isobutenyl complex (η^5-C_5H_5)Re(NO)(PPh_3)(CH=$C(CH_3)_2$) (**4**, 60% from **2b**), which in turn reacts with CH_3OSO_2F to give neopentylidene complex $[(\eta^5\text{-}C_5H_5)Re(NO)(PPh_3)(=CH(CH_3)_3)]^+FSO_3^-$ (90%). Complex **2a** and $Ph_3C^+PF_6^-$ react to give alkylidene complex $[(\eta^5\text{-}C_5H_5)Re(NO)(PPh_3)(=CHCH_2CPh_3)]^+PF_6^-$ (81%), which in turn reacts with *t*-BuO^-K^+ to give vinyl complex (*E*)-(η^5-C_5H_5)Re(NO)(PPh_3)(CH=CHCPh$_3$) (74%). Reactions of methoxycarbene complexes $[(\eta^5\text{-}C_5H_5)Re(NO)(PPh_3)(=C(OCH_3)CH_2R)]^+PF_6^-$ with NaH or DBU give α-methoxyvinyl complexes (*Z*)-(η^5-C_5H_5)Re(NO)(PPh_3)(C(OCH_3)=CHR) ((*Z*)-**10a,b,d,e** (R = C_6H_5)) in high yields. These are more nucleophilic than (*E*)-**2a-d** and react with alkyl iodides R'I to give methoxycarbene complexes $[(\eta^5\text{-}C_5H_5)Re(NO)(PPh_3)(=C(OCH_3)CHRR')]^+I^-$ that readily demethylate to acyl complexes (η^5-C_5H_5)Re(NO)(PPh_3)(COCHRR'). Thus, (*Z*)-**10b** and $C_6H_5CH_2Br$ react to give (*SR,RS*)-(η^5-C_5H_5)Re(NO)(PPh_3)(COCH(CH_3)($CH_2C_6H_5$)) ((*SR,RS*)-**13**; 71%), and (*Z*)-**10d** and CH_3I react to give (*SS,RR*)-**13** (88%; both diastereomers of ≥98% purity). Crystal structures of (*E*)-**2d** and (*Z*)-**10d** and extended Hückel MO calculations on Re-C_α rotamers of (η^5-C_5H_5)Re(NO)(PH_3)(CX=CH_2) (X = H, OH) are also described. Data are consistent with the following model for 1,3-asymmetric induction: electrophiles attack a Re-C_α rotamer with the ON-Re-C_α-C_β torsion angle (θ) close to 0° and on the C=C face opposite the bulky PPh_3 ligand.

Transition-metal complexes containing vinyl, or alkenyl, ligands, $L_nMCR{=}CR'R''$, have been known for some time and extensively studied.[3-8] However, as suggested by the paucity of review literature,[8] only recently have they attracted attention as a class

(1) University of Utah.

(2) University of Delaware.

0002-7863/87/1509-7688$01.50/0